

Pyrolysis Model for Mass Timber: B-RISK Theory

Colleen Wade

Project QR01810

Fire Research Group, funded by the Building Research Levy





Funded from the
Building Research Levy



1222 Moonshine Rd, RD1, Porirua 5381
Private Bag 50 908, Porirua 5240
New Zealand
branz.nz

© BRANZ 2021
ISSN: 2423-0839



Pyrolysis Model for Mass Timber: B-RISK Theory

FRG Report 2102009/1

16 July 2021



FRG Report 2102009/1

Pyrolysis Model for Mass Timber: B-RISK Theory

Prepared by:
Colleen Wade

Prepared for:
BRANZ Ltd.
Private Bag 50908
Porirua 5240

Project No: 2102009

16 July 2021



FRG, LEVEL 1 PWC CENTRE, 60 CASHEL ST, CHRISTCHURCH 8013, NEW ZEALAND



Quality Control

Revision	Date	Comment	Author	Reviewer
00	16 July 2021	Issue to client	C A Wade	G B Baker

©ALL RIGHTS RESERVED. FIRE RESEARCH GROUP LTD

This report (including any enclosures and attachments) has been prepared for the exclusive use and benefit of the client and solely for the purpose for which it is provided. Unless we provide express prior written consent, no part of this report should be reproduced, distributed or communicated to any third party. We do not accept any liability if this report is used for an alternative purpose from which it is intended, nor to any third party in respect of this report.

Table of Contents

1	Introduction	1
1.1	Background	1
1.2	Zone model	1
2	Pyrolysis of the moveable fire load	2
3	Heat transfer	5
3.1	Heat conduction model	5
3.2	Thermal boundary conditions	7
4	Thermophysical and related properties of wood and char	9
4.1	Heat of combustion of wood	10
4.2	Density	10
4.3	Dimensional changes in wood/char	10
4.4	Thermal conductivity	11
4.4.1	Wood	12
4.4.2	Char	13
4.5	Specific heat	14
4.5.1	Wood	14
4.5.2	Char	15
5	Kinetic pyrolysis submodel	15
5.1	Wood surface burning rate	15
5.2	Material kinetic properties	17
5.3	Model limitations	18
5.4	Calibration	19
6	Benchmarking	19
6.1	General	19
6.2	Pyrolysis model - decoupled	20
6.2.1	Constant heat flux experiments by Pope et al.	20
6.2.2	Furnace experiments by König and Walleij	20
6.3	Zone model - decoupled	24
6.3.1	Carleton University room fire experiments	24
6.3.2	NFPA Research Foundation room fire experiments	25
6.3.3	NRCC room fire experiments	28
6.4	Zone and pyrolysis model - coupled	30
6.4.1	NRCC room fire experiments	30
6.4.2	NFPA Research Foundation room fire experiments	30
6.5	Char depth validation	32
7	User guide	34
7.1	Instructions for the mass timber kinetic pyrolysis submodel	34
7.2	Calibration factor for the mass timber kinetic pyrolysis submodel	40
	References	41
	Appendices	46
A	Sensitivity of the post-flashover wood crib model in B-RISK to the plume entrainment algorithm used	47
B	Mass timber simple GE submodel	55
B.1	Description	55

B.2 Instructions for the mass timber simple GE submodel	56
---	----

List of Tables

Table 1	Kinetic parameters of materials, estimated using a genetic algorithm. . .	18
Table 2	Chemical composition of dry wood.	18
Table 3	Summary of key experimental parameters and model char depth predictions.	33

List of Figures

Figure 1	General arrangement of a wood crib.	4
Figure 2	Conceptual design fire	5
Figure 3	Schematic view of the finite difference scheme.	6
Figure 4	Photo of typical cracking that occurs in the charred surface of a laminated veneer lumber specimen subjected to radiant heat.	8
Figure 5	Flow chart for the moveable fire load coupled with the kinetic model for mass timber.	17
Figure 6	Laminated bamboo exposed to 60 kW/m ² with and without calibration.	21
Figure 7	Furnace time-temperature histories for experiments (from König and Walleij).	22
Figure 8	Depth of char due to standard fire resistance test exposure (König and Walleij – SFE Test Series A) compared with model prediction.	22
Figure 9	Depth of char due to standard fire resistance test exposure (König and Walleij – Test Series C1 to C3) compared with model prediction.	23
Figure 10	Depth of char due to standard fire resistance test exposure (König and Walleij – Test Series C4 to C6) compared with model prediction.	23
Figure 11	Measured and predicted total heat release rate for Carleton room fire experiments CLT fully protected with two layers of 12.7 mm thick gypsum board.	25
Figure 12	Measured and predicted enclosure gas temperatures for Carleton room fire experiments CLT fully protected with two layers of 12.7 mm thick gypsum board.	25
Figure 13	Measured and predicted total heat release rate for NFPA Research Foundation room fire Test 1-1 with CLT fully protected with three layers of 15.9 mm thick gypsum board.	26
Figure 14	Measured and predicted total heat release rate for NFPA Research Foundation room fire Test 1-1 with CLT fully protected with three layers of 15.9 mm thick gypsum board.	27
Figure 15	Measured and predicted total heat release rate for NFPA Research Foundation room fire Test 1-2 with CLT fully protected with two layers of 15.9 mm thick gypsum board.	28
Figure 16	Measured and predicted total heat release rate for NFPA Research Foundation room fire test 1-2 with CLT fully protected with two layers of 15.9 mm thick gypsum board.	28

Figure 17	Measured and predicted gas temperatures for room fire experiment 1 with CLT fully protected with three layers of gypsum board.	29
Figure 18	Enclosure Experiment 2 (33% walls and 10% ceiling exposed).	30
Figure 19	Enclosure Experiment 5 (35% walls and 100% ceiling exposed).	31
Figure 20	Enclosure Test 1-4 (100% ceiling only exposed).	31
Figure 21	Predicted versus experimentally determined char depth for the kinetic submodel, simple GE submodel and also including calculations using Brandon's method.	34
Figure 22	Example entry for a CLT material in the thermal database.	35
Figure 23	Room input parameters.	35
Figure 24	Menu selection for the mass timber pyrolysis model.	36
Figure 25	Parameters for the mass timber pyrolysis model.	36
Figure 26	Solver settings for the mass timber pyrolysis model.	37
Figure 27	Post flashover settings for the mass timber pyrolysis model.	38
Figure 28	Menu item to view graph of char depth output.	39
Figure 29	Graph of char depth output.	39
Figure 30	Changing the kinetic pyrolysis calibration factor.	40
Figure A.1	Mass flows in compartment with opening with vent mixing term.	47
Figure A.2	Plume entrainment, flaming region.	49
Figure A.3	Effect of plume flow on the layer height.	49
Figure A.4	Effect of plume flow on the heat release rate.	50
Figure A.5	Effect of plume flow on the calculated upper layer gas temperature.	51
Figure A.6	B-RISK Wall vent flow output with McCaffrey plume flow $\times 1.0$	52
Figure A.7	B-RISK Wall vent flow output with McCaffrey plume flow $\times 2.0$	52
Figure A.8	B-RISK Wall vent flow output with McCaffrey plume flow $\times 0.5$	52
Figure A.9	Flow schematic at 1000 s with McCaffrey plume flow $\times 1.0$	53
Figure A.10	Flow schematic at 1000 s with McCaffrey plume flow $\times 2.0$	53
Figure A.11	Flow schematic at 1000 s with McCaffrey plume flow $\times 0.5$	54
Figure B.1	Flow chart for the moveable fire load coupled with the simple GE sub-model for mass timber.	56
Figure B.2	Parameters for the mass timber simple GE model.	57

1. Introduction

1.1 Background

Design methods have been developed over recent years that attempt to predict the gas temperatures over the course of a fire that also include the contribution from the mass timber surfaces such as exposed cross-laminated timber (CLT) panels, as well as the incident heat flux to bounding surfaces and depth of char within such surfaces. Simpler methods include hand/spreadsheet calculations using parametric fire temperature equations and involve iterative processes to balance the char depth with the additional fuel contributed, such as the methods proposed by Barber et al. [1] and Brandon [2].

As a first step, Wade et al. [3] developed a post-flashover fire zone model based on energy and mass conservation within an enclosure bounded by mass timber elements by adapting the existing fire zone model B-RISK to include a simple wood pyrolysis model. This assumed a moveable fire load represented as wood cribs with the added contribution of fuel from the exposed timber surfaces incrementally added to the fire load at each time step. This was based on a one-dimensional heat transfer calculation for the timber surfaces to determine the depth of the 300 °C isotherm assuming constant thermal properties. Further information about this submodel is provided in [subsection B.1](#). Wade et al. [4] then developed a more advanced model with the timber surface pyrolysis determined from a four component (lignin, cellulose, hemicellulose and water) kinetic submodel where the thermal properties in the solid phase heat transfer analysis considered the different components of char and wood for each element considered.

Subsequently Wade [5] made further improvements by including modified thermal properties, dehydration and desorption effects, dimensional changes, and alternative kinetic properties. In all three model variations, a finite difference scheme was used to calculate heat transfer and internal temperatures within the exposed timber surfaces bounding the enclosure. Subsequent further changes [6] introduced an additional flame heat flux term for the burning timber surfaces that accounts for the oxygen mass fraction of the enclosure gases along with a critical mass loss rate for flaming combustion which better describes the thermal boundary conditions during the decay phase, especially as the enclosure oxygen levels return to their ambient value. However, it is apparent that a calibration of the pyrolysis model to compensate for phenomena still not otherwise addressed is nonetheless required in order to produce char depth predictions that are appropriate for design and ultimately to provide structural fire engineers with a more useful model to inform the fire design of mass timber buildings.

This report describes the theory and equations currently used in the model as at v2021.1, and presents benchmarking and char depth validation information.

1.2 Zone model

The two-zone model B-RISK is used considering both pre-flashover and post-flashover fire behaviour. The model is described more fully elsewhere [7] with some further key characteristics and modifications noted here.

Conservation of mass and energy leads to a set of first-order differential equations which allow the upper layer volume, upper and lower layer temperatures, and the pressure equation to be solved. The form of the equations is as given by Peacock et al. [8].

The mass flow of air and hot gases through the compartment wall opening is driven by buoyancy. Bernoulli's equation is used to calculate the mass flows generally following subroutines developed by Cooper and Forney [9, 10]. A near vent mixing correlation developed by Utiskul [11] has been applied where the incoming cold air behaves like a jet entering the vent with a characteristic velocity and diffusing downward because of buoyancy.

The strong plume model of Heskestad as described in ISO 16734 [12] for the buoyant plume is used for entrainment in the far field. For fully developed post-flashover fires where the entrainment height is small due to the layer height being close to the floor, the buoyant plume model is not appropriate (i.e. for near field entrainment). In this case the McCaffrey correlation for the flaming region is used [13]. When the fire is ventilation-limited, the oxygen-constrained heat release rate is used in the plume correlation instead of the well-ventilated free-burning heat release rate. This produces a plume flow that is in balance with the oxygen inflow through the openings (i.e. the mass flow of oxygen in the plume matches the mass flow of oxygen entering the compartment). Under these conditions, the energy balance for the upper layer control volume is not particularly sensitive to the total plume entrainment but is instead driven by the oxygen entering the compartment much like a one-zone well-stirred reactor. Therefore, the two-zone model is used for both the pre-flashover and post-flashover stages of the fire. Further analysis and supporting evidence for this is included in [Appendix A](#).

The model includes a four-wall radiation exchange algorithm following the method described by Forney [14]. This allows the ceiling, upper wall, lower wall and floor to transfer radiation independently between the different surfaces taking into account the absorption or blocking and emission of radiation by the gas-soot mixture. Radiant heating of these surfaces by the flames is also considered by treating the fire as a point source located centrally within the enclosure. The emission of radiation by soot particles and absorption by carbon dioxide and water vapour for both layers is included and used as an energy source term in the ordinary differential equations of the zone model. The fraction of energy passing through a soot-air mixture depends on the absorption coefficient of the soot and the path length through the gas. The absorption coefficient is approximated using the average extinction coefficient for the layer based on the concentration of soot in the gas layer. The soot yield is fuel-dependent and in the present study a value of 0.015 g/g for well ventilated flaming combustion of wood was used [15]. This yield is modified during the simulation based on the global equivalence ratio using a correlation developed by Tewarson et al. [16]. The radiation exchange submodel determines the net radiant heat flux emitted or absorbed by each room surface. These radiant fluxes are combined with the convective heat flux and used as the boundary condition for the surface heat conduction calculations.

2. Pyrolysis of the moveable fire load

During the initial growth period, before flashover and while the fire is well ventilated, the heat release and other characteristics supplied by the user for the item first ignited are used, with the mass loss rate given by:

$$\dot{m}_f = \frac{\dot{Q}}{\Delta H_c} \quad (1)$$

The initial fire growth rate is typically represented as $\dot{Q} = \alpha t^2$ where the α coefficient is selected according to the design fire growth rate for the preflashover fire. Following flashover a switch to a fully developed regime occurs where the remaining moveable fuel load is represented as wood cribs with the same total fire load in MJ as for the actual fire load (if different from wood cribs). Flashover is not a precise concept and criteria are usually based on the temperature at which the radiation from the hot gases in the compartment will readily ignite the combustible contents. Gas temperatures of 500–600°C are widely used [17] as a criterion. The flashover criterion recommended for this model is an average upper layer temperature of 500°C.

The fully-developed regime determines the fuel mass loss rate \dot{m}_f (kg/s) for two cases; a fuel surface area-controlled mass loss rate, and a ventilation-controlled mass loss rate. For the case of actual wood cribs being the fuel source a third case of porosity-control is also included.

The fuel surface area-controlled mass loss rate is given by Equation 2 representing crib fires [18] (see Figure 1) where D (m) is a characteristic fuel or stick thickness, v_p (m/s) is a surface regression rate - for wood taken as $0.0000022D^{-0.6}$, m (kg) is the mass of fuel remaining and m_{init} (kg) is the original mass of fuel (determined using the specified floor area and fuel load energy per unit floor area). This equation assumes cribs are ignited instantaneously.

$$\dot{m}_f = \frac{4}{D} m_{init} v_p \sqrt{\frac{m}{m_{init}}} \quad (2)$$

The mass loss rate for crib porosity-controlled burning is given by Equation 3 where S is the stick spacing (m) and H_c is the crib height (m).

$$\dot{m}_f = 4.4 \times 10^{-4} \frac{S}{H_c} \frac{m_{init}}{D} \quad (3)$$

The burning rate for ventilation-controlled condition is given by Equation 4 where $13100\dot{m}_p Y_{O_2,l}$ is the maximum rate of heat release (kW) that can be supported by the oxygen in the plume flow and ΔH_c (kJ/kg) is the heat of combustion of the fuel. The constant (13100) in Equation 4 is the oxygen calorimetry constant representing the energy released per unit mass of oxygen consumed (in kJ/kg) and is applicable to a wide range of common fuels [18, 19]. Assuming the oxygen flow in the plume represents the total available oxygen for combustion is a more generally applied method for a two-zone model compared to calculating the oxygen inflow through a single opening from the outside and can also be used where there are multiple openings or where other rooms are connected to the room of fire origin.

$$\dot{m}_b = \frac{13100\dot{m}_p Y_{O_2,l}}{\Delta H_c} \quad (4)$$

This burning rate corresponds to that able to burn inside the room given the available oxygen and is not necessarily the total mass loss rate of the wood cribs. For the ventilation controlled case, the mass loss rate is then multiplied by Ω - a user-defined input that can be used to specify the ratio between the burning rate and the mass loss rate of the movable fire load under ventilation controlled conditions as given by Equation 5, where $\Omega = 1$ corresponds to a mass loss rate equal to the burning rate inside the enclosure. Ω also corresponds to the global equivalence ratio as defined by Pitts [20].

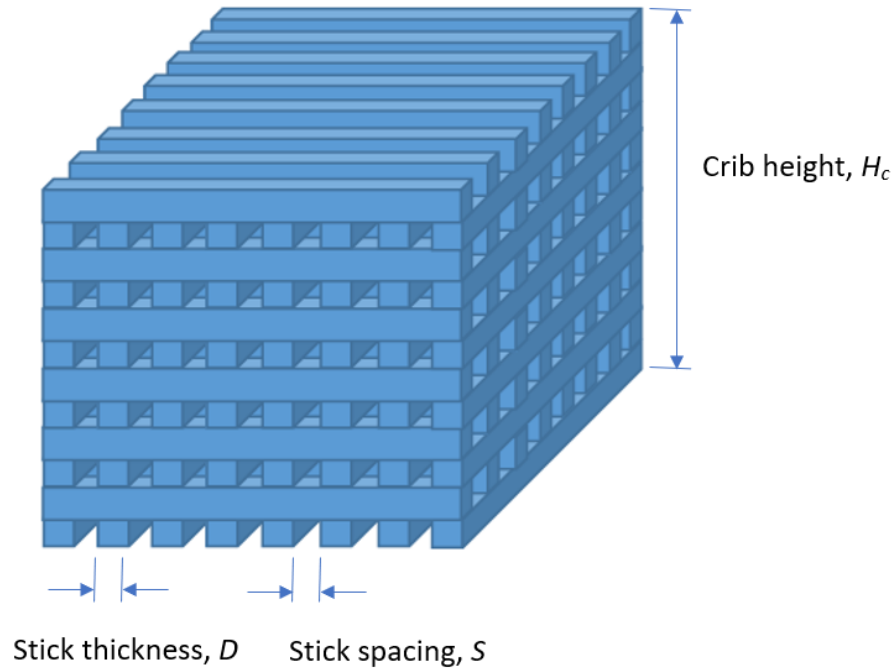


Figure 1. General arrangement of a wood crib.

$$\Omega = \frac{\dot{m}_{f,tot}}{\dot{m}_b} = \frac{\Delta H_c \dot{m}_{f,tot}}{13100 \dot{m}_p Y_{O_2,l}} \quad (5)$$

This means the user is effectively specifying the global equivalence ratio (GER) as it determines the relative proportion of gasified fuel burning inside and outside the room. $\Omega = 1$ corresponds to all the fuel generated actually burning within the room to match the available oxygen with $\Omega = 1.3$ used as a default value for wood cribs in a non-combustible or protected-timber compartment. It has been observed experimentally that wood cribs do not burn more than 30 to 40% fuel rich, with Babrauskas reporting an upper limit of approximately 37% fuel rich ($\Omega = 1.37$) [18]. Since enclosure effects on the mass loss rate of the cribs is not included here, this approach gives the user more control over the burning regime and can be used to provide a closer match to experimental observations of external flaming. This user input (Ω) to the post-flashover fire model will be referred to as GER or GE in this report. The governing burning rate inside the enclosure is taken as the lesser of the fuel-controlled, porosity-controlled and ventilation-controlled rates.

B-RISK keeps track of the total amount of fuel (moveable fire load) consumed during the simulation and when all the fuel is consumed (based on the user supplied input for the FLED and the enclosure floor area) the mass loss rate then becomes zero. An illustration of the general form of the design fire is shown in Figure 2. The inclusion of additional fuel contributed by any exposed mass timber panels is discussed later in [subsection 5.1](#).

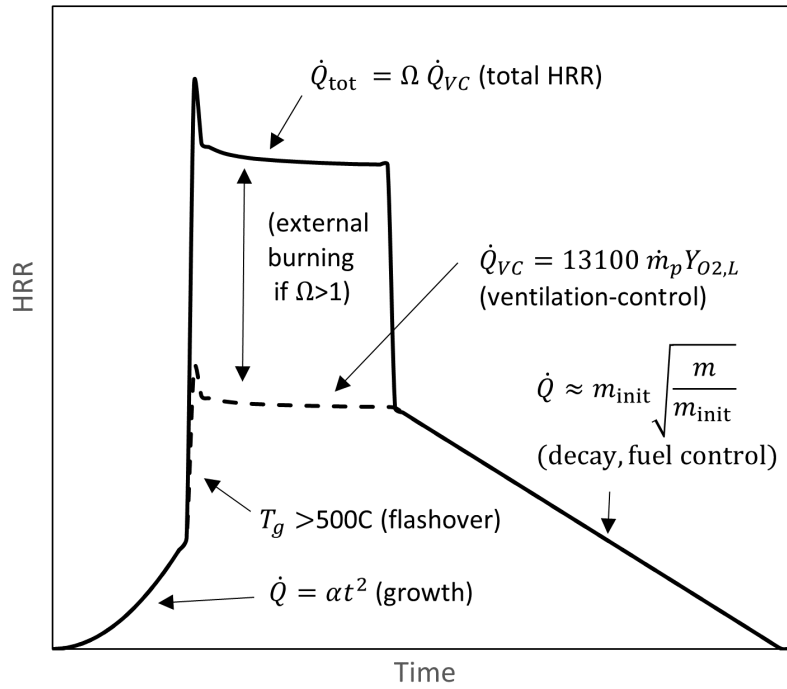


Figure 2. Conceptual design fire.

3. Heat transfer

3.1 Heat conduction model

An implicit one-dimensional, finite-difference scheme is used to calculate heat conduction through the ceiling, walls and floor of the compartment. A schematic view of the finite difference scheme is shown in [Figure 3](#). This allows the temperature at any internal node to be calculated by solving a set of simultaneous equations for the unknown nodal temperatures at each time step. Under transient conditions with constant properties and no internal generation the appropriate form of the heat equation for a one-dimensional system is [\[21\]](#):

$$\frac{1}{b} \frac{\partial T}{\partial t} = \frac{\partial^2 T}{\partial x^2} \quad (6)$$

The finite difference approximation of the time derivative can be expressed by [Equation 7](#) with the m subscript denoting the x location of the nodal points and the superscript p used to denote the time dependence such that the time derivative is stated in terms of the difference in temperature associated with the new $(p+1)$ timestep and that at the previous p timestep [\[21\]](#).

$$\left. \frac{\partial T}{\partial t} \right|_m \approx \frac{T_m^{p+1} - T_m^p}{\delta t} \quad (7)$$

The temperature at each node is calculated by solving a set of simultaneous equations for the unknown nodal temperatures at each time step [\[21\]](#). The implicit form of the one-

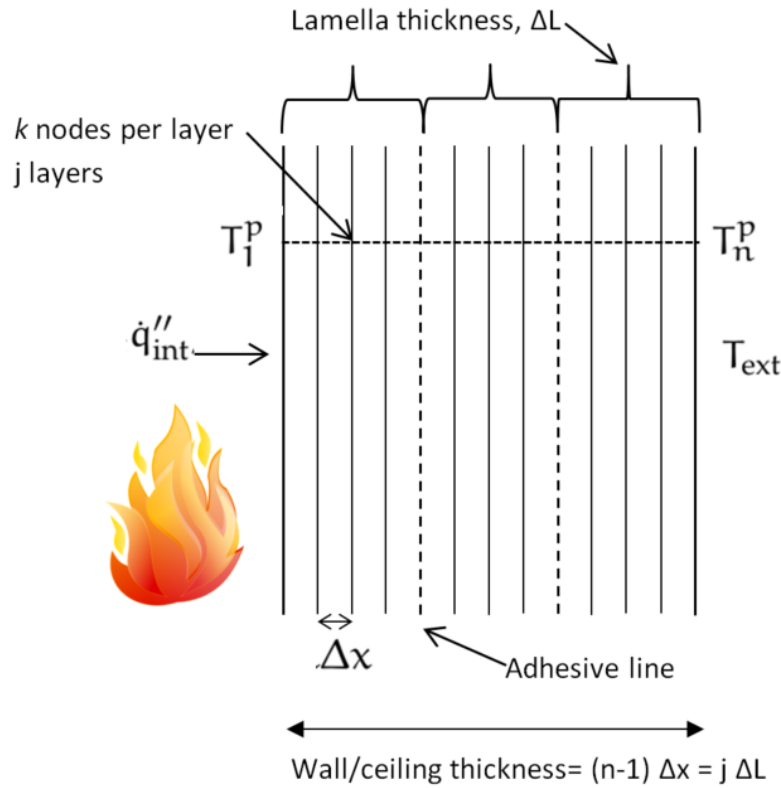


Figure 3. Schematic view of the finite difference scheme.

dimensional finite-difference scheme for a surface node is given by Incropera and deWitt [21] as:

$$(1 + 2Fo)T_1^{p+1} - 2FoT_2^{p+1} = \frac{2Fo \text{ Bi} \dot{q}_{\text{int}}''}{h_c} + T_1^p \quad (8)$$

Where \dot{q}_{int}'' is the incident heat flux to the exposed surface and the Fourier and Biot numbers are given by:

$$Fo = \frac{b\Delta t}{(\Delta x)^2} \text{ with } b = \frac{k}{\rho c_p} \quad (9)$$

$$\text{Bi} = \frac{h\Delta x}{k} \quad (10)$$

The implicit form for an interior node is given as:

$$-FoT_{m-1}^{p+1} + (1 + 2Fo)T_m^{p+1} - FoT_{m+1}^{p+1} = T_m^p \quad (11)$$

Writing an equation for each node gives n equations which must be solved simultaneously for each timestep. This is done using the matrix inversion method by expressing the equations in the form $[A][T]=[C]$, where:

$$[A] = \begin{bmatrix} 1 + 2Fo & -2Fo & 0 & 0 & \dots & 0 \\ -Fo & 1 + 2Fo & -Fo & 0 & \dots & 0 \\ 0 & -Fo & 1 + 2Fo & -Fo & \dots & 0 \\ \vdots & \vdots & \ddots & \dots & \dots & \vdots \\ 0 & \dots & \dots & 0 & -2Fo & 1 + 2Fo \end{bmatrix} \quad (12)$$

$$[C] = \begin{bmatrix} 2FoBi_{\text{int}}\ddot{q}_{\text{int}}''/h_c + T_1^p \\ T_2^p \\ T_3^p \\ \vdots \\ 2FoBi_{\text{ext}}(T_{\text{ext}} - T_n^p) + T_n^p \end{bmatrix} \quad (13)$$

While the simplest form of the heat conduction equation is shown here with constant properties and no internal generation as assumed in the existing B-RISK zone model, for the calculations for wood pyrolysis discussed later in this chapter temperature-dependent properties have been introduced for the mass timber panels. However, constant properties have been assumed for the non-participating surfaces including the floor and plasterboard protected surfaces which should ideally be corrected in future work.

A limitation of the one-dimensional analysis is that it does not account for any cracking that occurs in the char (see [Figure 4](#)) which increases the relative importance of radiative heat transfer through the char pores and reduces the importance of in-depth conduction into the solid [22]. This potentially compromises the assumptions described in this section, and remains an area of possible further research.

3.2 Thermal boundary conditions

Heat transfer to solid surfaces exposed to fire comprises convection and radiation components. The total net heat flux to a solid surface is given by [23]:

$$\dot{q}_{\text{total}}'' = \dot{q}_{\text{rad}}'' + \dot{q}_{\text{con}}'' \quad (14)$$

Ignoring any reflected radiation, the net radiant contribution is given as the difference between the absorbed radiation and the reradiated or emitted radiation from the surface.

$$\dot{q}_{\text{rad}}'' = \dot{q}_{\text{abs}}'' - \dot{q}_{\text{emi}}'' = \alpha \dot{q}_{\text{inc}}'' - \epsilon \sigma T_s^4 \quad (15)$$

Applying Kirchhoff's Law with $\alpha = \epsilon$ gives:

$$\dot{q}_{\text{rad}}'' = \epsilon (\dot{q}_{\text{inc}}'' - \sigma T_s^4) \quad (16)$$

The incident radiant flux striking an enclosure surface \dot{q}_{inc}'' comes from several sources and is in general a complicated term involving contributions due to radiation from the fire plume (point source assumption), radiant exchange contributions from other surfaces in the enclosure (depends on view factors and absorption/transmission by the gas layers separating the surfaces) and emission from the gas layers to the surface (including emission by soot particles and absorption by CO_2 and H_2O). B-RISK uses a 4-wall radiation model assuming a rectangular shaped enclosure where the ceiling, upper wall, lower wall and floor are considered separate entities and heat transfer is calculated to each one. The



Figure 4. Photo of typical cracking that occurs in the charred surface of a laminated veneer lumber specimen subjected to radiant heat.

incident radiant heat flux is calculated by the fire model (B-RISK) and in general terms is given by:

$$\epsilon \dot{q}_{\text{inc}}'' = \sum_i (\epsilon_i F_i \sigma T_i^4) \quad (17)$$

Where the subscript i refers to the various surfaces and source terms contributing to the incident radiation striking a surface.

An additional radiation term, \dot{q}_f'' , is introduced to the boundary conditions for the heat transfer to the enclosure surface being a flame heat flux term for burning timber wall and ceiling surfaces where the heat flux from the flames is estimated from Equation 18 after Rasbash et al. [24], where \dot{m}'' is the mass loss rate per unit area from the burning timber surface (calculated from the pyrolysis model described later), $\Delta H_{c,n}$ is the heat of combustion of the timber (taken as 17.5 MJ/kg) and ϕ is the proportion of energy from the flames transferred back to the surface and estimated from Equation 19 [24] where h_c is the convective heat transfer coefficient (in W/m²K), $c_{p,\text{air}}$ is the specific heat of air (1.01 J/gK), Y_{ox} is the oxygen mass fraction (0.23 at ambient) but calculated by the zone model for the upper layer gases in the enclosure fire and r is the stoichiometric ratio of oxygen to fuel taken as 3.43 for timber [24].

$$\dot{q}_f'' = \phi \Delta H_{c,n} \dot{m}'' \quad (18)$$

$$\dot{m}_{cr}'' = \frac{h_c}{c_{p,\text{air}}} \ln \left(1 + \frac{Y_{\text{ox}}}{r\phi} \right) \quad (19)$$

Taking the critical mass loss rate (\dot{m}_{crit}'') for timber as 3.5 g/m²s from Bartlett [8] and combining Equation 18 and Equation 19 gives the following expression for the flame heat flux:

$$\dot{q}_f'' = \frac{Y_{\text{ox}} \Delta H_{c,n} \dot{m}''}{r \left[\exp \left(\frac{c_{p,\text{air}} \dot{m}_{\text{crit}}''}{h_c} \right) - 1 \right]} \quad (20)$$

Including the flame flux into the net radiation, Equation 16 is modified to give:

$$\dot{q}_{\text{rad}}'' = \epsilon (\dot{q}_{\text{inc}}'' + \dot{q}_f'' - \sigma T_s^4) \quad (21)$$

The convective heat flux depends on the difference between the surrounding gas temperature and the surface temperature and can be written as:

$$\dot{q}_{\text{con}}'' = h_c (T_g - T_s) \quad (22)$$

where h_c is the heat transfer coefficient, T_s is the temperature of the exposed surface and T_g the gas temperature adjacent to the exposed surface.

In B-RISK, the interior convection coefficient (h_c) used in the convective heat transfer calculations between the gas layer and the room surface are by default calculated following the method described by Peacock et al. [25] assuming natural convection, however for simulations of fire in mass timber compartments a constant convection coefficient of 50 W/m²K has been used as discussed below.

Bartlett [26] conducted bench scale experiments using the Fire Propagation Apparatus (FPA) and evaluated $c_{p,\text{air}}/h_c$ to be 9 g/m²s for a flat plate while Rasbash et al. assumed 10 g/m²s [24]. EN 1991-1-2 gives the convective heat transfer coefficient for the standard fire resistance test exposure as 25 W/m²K. Veloo and Quintiere [27] studied the convective heat transfer coefficient in fully developed fire experiments, using a heated plate heat flux gauge and a water-cooled gauge, in which the convective heat transfer coefficient was measured and correlated over a range of temperatures in flaming and cooling periods for enclosure fires. They found the heat flux could attain levels between 100 and 200 kW/m² where convection accounted for up to 25%, with an order of magnitude difference for the convective heat transfer coefficient being as high as 50 W/m²K. Higher convective heat flux values are attributed due to high local velocities disturbing the flow field [28]. Given the findings by Veloo and Quintiere [27] and also by Gorska et al. [29], who observed higher velocities at the opening that they attributed to the burning timber surfaces producing stronger buoyant gas flows inside the enclosure, in the present paper, a constant post-flashover convective heat transfer coefficient (h_c) of 50 W/m²K has been used both for the zone model calculations and for evaluating the flame flux for burning timber surfaces from Equation 20. This value is likely at the upper end of the range, but provides a more conservative estimate of the heat transfer to the mass timber surfaces during the decay period in particular.

4. Thermophysical and related properties of wood and char

Thermophysical and related properties of wood and char for use in the pyrolysis model for the mass timber panels are presented in this section. Different properties for the wood and char are used.

4.1 Heat of combustion of wood

Gross heat of combustion values are measured in a bomb calorimeter resulting in typical values of around 20 MJ/m² for oven dry wood [30] for complete combustion of the wood and char. The actual heat of combustion observed in real fires is not the gross value. Spearpoint and Quintiere [31] discuss the heat of combustion of wood where the main constituent of wood char is carbon and the net heat of combustion for a carbon and oxygen to carbon dioxide reaction is 32 MJ/kg. Given that the average net heat of combustion of wood for a complete reaction is 17 MJ/kg and assuming a typical char yield for dry wood of 1/3 by mass allows the mean heat of combustion of the wood volatiles during the flaming stage ($\Delta H_{c,fl}$) to be solved following Equation 23.

$$1/3(32) + 2/3(\Delta H_{c,fl}) = 17 \quad (23)$$

This gives a value of 10 MJ/kg for the heat of combustion of the wood volatiles during the flaming stage ($\Delta H_{c,fl}$). Spearpoint and Quintiere [31] concluded that only about 60% of the energy of wood is released during the flaming stage of combustion. Using the same methodology with assumed char yields of 0.25 and 0.20 give 12 MJ/kg and 13.3 MJ/kg for the respective values of heat of combustion of the wood volatiles during the flaming stage.

Eurocode 5 [32] specifies a constant heat of combustion for wood of 17.5 MJ/kg but with an assumed combustion efficiency of 0.8, giving an effective heat of combustion value of 14 MJ/kg. This value has generally been used in all subsequent analysis presented in the following sections of this report.

4.2 Density

The density of oven-dry wood depends on species and is typically in the range 320 to 720 kg/m³ [33]. Given a wood density value ρ_w at ambient with moisture content u and ignoring any expansion term, the oven dry density can be given by Equation 24 [34].

$$\rho_{w,dry} = \frac{\rho_w}{(1 + u)} \quad (24)$$

An element within the cross section of the mass timber panels may comprise water, char and solid at any given time and temperature. The pyrolysis solver calculates the residual mass fraction of each of the components such that as pyrolysis proceeds the total residual mass of the element is the sum of the residual mass of the components and this reduces as the reaction proceeds. The apparent density is that fraction of the original density at a given time. When all the water and solids have completely pyrolysed, only the residual char fraction remains.

A further correction to the apparent density to account for dimensional changes as described in the next section is then made.

4.3 Dimensional changes in wood/char

The mass of wood changes as it dries and loses moisture, and as wood is converted to char. The volume also changes as the wood shrinks due to this moisture loss and charring. During fire exposure, the exposed wood surface also typically recedes as the combustion progresses due to the char contraction and char oxidation [34].

Since the model described here relies on finite difference calculations with a fixed grid, dimensional changes due to drying and thermal expansion are accounted for by making a correction to the density and thermal conductivity.

Janssens [34, 35] gives the apparent density of the wood/char (Equation 25) as a function of the residual mass Z at a given time, the oven-dry density of wood $\rho_{w,dry}$ and dimensional changes due to drying and thermal expansion. f_l , f_r , f_t are the thermal expansion factors for softwoods in the longitudinal, radial and tangential directions respectively. T is the temperature and T_r is a reference temperature taken as 20°C.

$$\rho_{w,corrected} = \frac{Z}{f_l f_p^2} \rho_{w,dry} \quad (25)$$

$$f_l = 1 + 3.75 \times 10^{-6} (T - T_r) \quad (26)$$

$$f_r = 1 + \rho_{w,dry} \times 55 \times 10^{-9} (T - T_r) \quad (27)$$

$$f_t = 1 + \rho_{w,dry} \times 82 \times 10^{-9} (T - T_r) \quad (28)$$

An average expansion factor perpendicular to the grain, and also including a factor for expansion due to moisture is given in Equation 29 and used in Equation 25.

$$f_p = \sqrt{f_r f_t} \sqrt{1 + 0.00084 \rho_{w,dry} u} \quad (29)$$

A correction to the thermal conductivity k (Equation 32) is made using the average char contraction factor for the radial and tangential directions respectively from the following expressions given by Parker [36].

$$f_r = 1 - 0.64 \times (1 - (Z + u))^3 \quad (30)$$

$$f_t = 1 - 0.45 \times (1 - (Z + u))^{3/2} \quad (31)$$

$$k_{corrected} = \frac{2k}{(f_r + f_t)} \quad (32)$$

4.4 Thermal conductivity

Thermal conductivity of wood generally increases with temperature, moisture content and density. Wood is also anisotropic and thermal conductivity along the grain may be 1.5 to 2.8 times the conductivity across the grain [37].

Janssens and Douglas [34] provide detailed equations for the thermal conductivity of wood, char and partially charred wood at ambient and elevated temperature. These equations have been adopted for the current model as described in the following sections.

At each time step, the pyrolysis model provides the mass fraction of wood (lignin, hemicellulose, cellulose), water and char comprising each element within the depth of the mass timber. The overall effective thermal conductivity applying to each element is weighted based on the relative proportion of wood and char at any given time and using

the values of thermal conductivity calculated for the wood and char from [Equation 45](#) and [Equation 54](#) respectively.

4.4.1 Wood

An upper limit for thermal conductivity of wood k_{\max} is obtained for a system with the same porosity, composed of alternating air and solid layers arranged in parallel.

$$k_{\max} = \pi_s k_s + \pi_w k_w + \pi_g k_g \quad (33)$$

where π_s is the fraction of total volume of wood occupied by wood fibers in m^3/m^3 given by:

$$\pi_s = \frac{\rho_{w,dry}}{(1 + 0.00084\rho_{w,dry}u)\rho_s} \quad (34)$$

where $\rho_{w,dry}$ is the oven-dry density of the wood with the bulk density ρ_s equal to $1460 \text{ kg}/\text{m}^3$.

k_s is the thermal conductivity of wood fiber, $\text{W}/\text{m}\cdot^\circ\text{C}$ given by [Equation 35](#) with a reference temperature T_r of 20°C .

$$k_s = 0.42 + 0.0013(T - T_r) \quad (35)$$

k_w is the thermal conductivity of bound water taken as $0.8 \text{ W}/\text{mK}$, π_w is the fraction of the total volume of wood occupied by bound water, m^3/m^3 from [Equation 36](#) and the density of bound water ρ_w given by [Equation 37](#).

$$\pi_w = \frac{\rho_{w,dry}u}{(1 + 0.00084\rho_{w,dry}u)\rho_w} \quad (36)$$

$$\rho_w = 1298 - 1132u + 1766u^2 \quad (37)$$

k_g is the thermal conductivity of the gas filling the void spaces, $\text{W}/\text{m}\cdot^\circ\text{C}$ given as a function of temperature, T in $^\circ\text{C}$, by [Equation 38](#) based on literature data.

$$k_g = 0.024 + 7.05 \times 10^{-5}T - 1.59 \times 10^{-8}T^2 \quad (38)$$

Wood is assumed to consist of solid fibre in the cell walls, and air in the cell cavities. Porosity π_g is the fraction of the total volume occupied by air and is given by:

$$\pi_g = 1 - \pi_s - \pi_w \quad (39)$$

A lower limit k_{\min} is obtained for a system of layers in series.

$$k_{\min} = \frac{k_g k_s k_w}{\pi_g k_s k_w + \pi_s k_g k_w + \pi_w k_s k_g} \quad (40)$$

The real value of thermal conductivity of the wood (k) falls between these upper and lower limits and can be obtained as a weighted average with weighing factor ξ using [Equation 41](#) and [Equation 43](#).

$$\xi = 0.58 + 10^{-4} \rho_{w,dry} + 0.5u \quad (41)$$

$$k1 = \xi k_{max} + (1 - \xi) k_{min} + k_r \quad (42)$$

where k_r is a term added to account for radiative heat transfer in the cell cavities.

$$k_r = \frac{4\pi_g \sigma (T + 273)^3 d_p}{1 - \pi_g} \quad (43)$$

where d_p is the average diameter of the cell cavity, m given by Equation 44.

$$d_p = 3.5 \times 10^{-5} \sqrt{\pi_g} \quad (44)$$

Following Janssens and Douglas [34], a further temperature dependency correction is made such that the thermal conductivity of the oven dry wood at temperature T is given by:

$$k_o(T) = \frac{k1 \rho_o(T) c_o(T)}{\rho_o(T_r) c_o(T_r)} \quad (45)$$

where $c_o(T)/c_o(T_r)$ is the ratio of the specific heat using Equation 57 and $\rho_o(T)/\rho_o(T_r)$ is the ratio of the density using Equation 25.

4.4.2 Char

Janssens and Douglas [34] also provide similar equations for the thermal conductivity of the char but excluding the water component, and with the properties used here being non-reversible such that the property is based on the maximum temperature reached, T_{max} .

$$k_{max} = \pi_s k_s + \pi_g k_g \quad (46)$$

$$\pi_s = \rho_{w,dry} / \rho_s \quad (47)$$

where $\rho_s = 1305 \text{ kg/m}^3$ is the bulk density of char taken at 600 °C [34].

$$\pi_g = 1 - \pi - s \quad (48)$$

$$k_s = 0.33 + 0.00016 T_{max} + 0.000000108 T_{max}^2 \quad (49)$$

$$k_g = 0.024 + 0.0000705 T_{max} - 0.0000000159 T_{max}^2 \quad (50)$$

$$k_{min} = \frac{k_g k_s}{(\pi_g k_s + \pi_s k_g)} \quad (51)$$

$$dp = 0.000035 \sqrt{\pi_g} \quad (52)$$

$$k_r = 4\pi_g \sigma (T_{\max}^3) dp / (1 - \pi_g) \quad (53)$$

The thermal conductivity of the char is given by:

$$k_2 = \xi k_{\max} + (1 - \xi) k_{\min} + k_r \quad (54)$$

where, the weighing factor ξ is given by:

$$\xi = 0.58 + 0.0001 \rho_{w,dry} \quad (55)$$

4.5 Specific heat

The overall effective specific heat applying to each element is weighted based on the relative proportion of wood and char at any given time and using the values of specific heat calculated for the wood from Equation 56, with latent heat of vaporisation (Equation 61) and heat of wetting (Equation 62) added, and with the specific heat of char from Equation 63.

4.5.1 Wood

Specific heat depends on temperature and moisture content but not on density or species [38]. Janssens and Douglas give the specific heat of wood at temperature, T in °C and moisture content fraction u based on extensive surveys of wood from the literature.

$$c_u(T) = \frac{c_o(T) + 4187u}{1 + u} + \Delta c(T, u) \quad (56)$$

with

$$c_o(T) = 1159 + 3.86T \quad (57)$$

and

$$\Delta c(T, u) = (23.55T - 1326u + 2417)u \quad (58)$$

where: $c_u(T)$ is the specific heat of wood with moisture content u at temperature T , in J/(kg °C); $\Delta c(T, u)$ is a correction term in J/(kg °C) and accounts for the water bound to the cell walls; and $c_o(T)$ is the specific heat of oven dry wood at temperature T in J/(kg °C).

Janssens and Douglas [34] give the heat of vaporisation of water in kJ/kg of water as a function of temperature in °C as:

$$\Delta h_v = 2552 - 2.93T \quad (59)$$

They also give the integral heat of wetting in kJ/kg of water as:

$$\Delta h_w = \frac{92.1}{0.07 + u} \quad (60)$$

These enthalpy terms can either be accounted for directly in the heat transfer calculations or they can be included within the temperature dependent specific heat equations over a defined temperature range (e.g. 100 - 120°C). Here, in the temperature range 100 to 120 °C, while the temperature is increasing, terms for the latent heat of vaporisation, and for the heat of wetting are added.

Using the midpoint temperature of 110 °C and assuming the water is evaporated over the 20 °C range from 100 to 120 °C, Δh_v is reformulated in kJ/(°C) per kg of wood as:

$$\Delta h'_v = [2552 - (2.93 \times 110)]u/20 \quad (61)$$

Similarly, the integral heat of wetting in kJ/(°C) per kg of wood is given as:

$$\Delta h'_w = \frac{92.1u}{20(0.07 + u)} \quad (62)$$

4.5.2 Char

Janssens and Douglas [34] give the specific heat for wood char in Equation 63 with temperature units in °C.

$$c_c = 714 + 2.3(T) - 8 \times 10^{-4}(T)^2 - 3.7 \times 10^{-7}(T)^3 \quad (63)$$

5. Kinetic pyrolysis submodel

5.1 Wood surface burning rate

In this wood pyrolysis submodel, the decomposition of solid wood is described by an Arrhenius equation that gives a relationship between the reaction rate and temperature of the solid. This requires the kinetic properties - activation energy E_i , pre-exponential factor A_i and reaction order n_i (also known as the kinetic triplet) to be specified to determine the decomposition rate. A multiple-component scheme is used that assumes a solid material is composed of several components with each component undergoing a single independent reaction to generate products [39]. The constituent components of solid wood included in the model are cellulose, hemicellulose, lignin and water. The reaction rate for each component $w_{i,j}$ at a given time can be described with a first order differential equation where $Y_{i,j}$ is the mass fraction ($m_i/m_{i,init}$) of component i at time j , m_i is the mass of component i and $m_{i,init}$ is the initial mass of component i . For each component the initial mass fraction is $Y_{i,init} = 1$ at the start of the simulation. c_i is the initial fraction of the overall unheated composite solid represented by component i i.e. $m_{i,init}/m_{init}$. Equation 64 is solved using numerical methods to give the value of Y_i at each time step.

$$w_{i,j} = \frac{dY_{i,j}}{dt} = c_i A_i \exp\left(-\frac{E_i}{RT_{i,j}}\right) (Y_{i,j})^{n_i} \quad (64)$$

The solid is represented by the one-dimensional finite difference scheme illustrated previously in Figure 3 and the overall reaction rate at a given time is the sum of the reaction rates of all the components within a given layer or slice of the solid material at a given temperature. The mass loss rate is derived from the reaction rates for each layer and

summed over all the layers to give a total reaction rate for the wood material at a given time as described next.

For the cellulose, hemicellulose and lignin components, a char residue yield ν_i is specified with the mass fraction of char $X_{i,j}$ at time j given by Equation 65 and Equation 66.

$$X_{i,j} = (1 - Y_{i,j})\nu_i \quad (65)$$

The mass fraction of char residue at time j for each layer and for the three components (excluding moisture/water) is:

$$X_j = \sum_{i=1}^3 (X_{i,j}c_i) = \sum_{i=1}^3 ((1 - Y_{i,j})\nu_i c_i) \quad (66)$$

At a given time j , the mass of solid wood that remains per unit volume is given by Equation 67 where ρ_{init} is the initial density of wood.

$$m_j''' = \sum_{i=1}^3 (Y_{i,j}c_i\rho_{\text{init}}) \quad (67)$$

The total mass loss rate in kg/(m³s) can then be given by:

$$\frac{dm}{dt} = -\frac{(m_j - m_{j-1})}{\Delta t} \quad (68)$$

Ignoring any char oxidation, the gasification rate of fuel available to be converted to combustion energy in the fire model ($\dot{m}_{s,j}$) in a single layer of the finite difference scheme is given by:

$$\frac{dm_{s,j}}{dt} = -\frac{(m_{s,j} - m_{s,j-1})}{\Delta t} \quad (69)$$

At each time step this can be summed over all the layers (L=1 to N) in the finite difference scheme as per Equation 70 where Δx is the thickness of each layer, assuming that the gases are instantly transported to the fire-exposed surface of the material where they may burn.

$$\dot{m}_j'' = \sum_{L=1}^N \left(\sum_{i=1}^3 (Y_{i,j} - Y_{i,j-1}) c_i \rho_{\text{init}} \Delta x \right) \quad (70)$$

The rate of heat release (\dot{Q}'') from the combustible gases determined from the mass flux (\dot{m}'') and the heat of combustion ΔH_c is given by Equation 71 adapted from Wang et al. [40] with the temperatures inside the solid found using a one-dimensional heat conduction equation to compute the solid phase temperature gradient at x depth.

$$\dot{Q}'' = \Delta H_c \dot{m}'' = \Delta H_c \rho_{\text{init}} \int_{L=1}^N \sum_{i=1}^3 (1 - \nu_i) A_i \left(\frac{\rho_i}{\rho_{\text{init}}} \right)^{n_i} \exp \left(\frac{-E_i}{RT(x)} \right) dx \quad (71)$$

A flow chart illustrating the coupling of moveable fire load and the contribution of the mass timber when the kinetic submodel is used is shown in Figure 5.

COMPONENT	E_i (J/mol)	A_i (s ⁻¹)	n_i	RESIDUE
Hemicellulose	1.64×10^5	5.78×10^{13}	4.166	0.268
Cellulose	1.95×10^5	2.68×10^{14}	0.85	0.1
Lignin	1.38×10^5	2.18×10^{10}	7.0	0.567
Water	1.62×10^5	1.0×10^{20}	1.0	0

Table 1. Kinetic parameters of materials, estimated using a genetic algorithm [41].

TYPE OF WOOD	CELLULOSE (%)	HEMICELLULOSE (%)	LIGNIN (%)
Hardwood	40-44	23-40	18-25
Softwood	40-44	20-32	25-35

Table 2. Chemical composition of dry wood [34].

Richter et al. [43] found that variations in kinetics had only a small effect ($\pm 1 \text{ gm}^{-2}\text{s}^{-1}$) on the predicted mass loss rate at both the microscale (mg-samples) and mesoscale (kg-samples) and to have a negligible effect on the predicted temperatures ($\pm 16 \text{ K}$) across different depths, heat fluxes and oxygen concentrations at the mesoscale. They stated that the variation in kinetics is negligible for predicting charring across scales and a kinetic model of charring derived for one wood species should be valid for all wood species [43].

The mass of water that remains at a given time j per unit volume can be expressed by Equation 72 where $Y_{\text{water},j}$ is determined by solving Equation 64 for water as the component i .

$$m_{\text{water},j} = Y_{\text{water},j} c_{\text{water}} \rho_{\text{init}} \quad (72)$$

The mass of char present at a given time per unit volume is:

$$m_{\text{c},j} = X_j \rho_{\text{init}} \quad (73)$$

The total mass present at a given time per unit volume (which is also the apparent density of the material) is therefore:

$$m_j = m_{\text{s},j} + m_{\text{water},j} + m_{\text{c},j} \quad (74)$$

5.3 Model limitations

Despite addressing a wide range of phenomena in the pyrolysis model, not all those that may be important are captured, leading to the ultimate char depth predictions generally being underestimated in the absence of any calibration. The most significant phenomena or other effects not addressed in the pyrolysis submodel are:

- Oxidation of the char.
- Cracking and continued degradation or erosion of the wood char during the decay phase such that in reality the char rate is greater than expected during the decay.

- Water vapour within the timber panels evaporating but then condensing again deeper into the enclosure surfaces.
- Where exposed wood surfaces are oriented to face each other, reradiation between the surfaces may prolong the burning and result in greater charring.

Furthermore, the zone model formulation may also not correctly capture effects such as:

- The actual mass loss rate for the wood cribs (representing the moveable fire load) may differ from the assumed burning rate given by correlations rate due to the enclosure heating and ventilation effects, collapsing cribs or other reasons.
- Representing actual fuel packages and materials as wood cribs may not be realistic.
- Not accurately representing the conduction heat losses within the enclosure due to the thermal properties applying to the partial areas protected with gypsum plaster-board being represented by the properties of wood/char.
- Although B-RISK is a multi-room model, the mass timber pyrolysis model has only been developed considering a single enclosure, and has not been tested and is therefore not currently recommended for use as part of a multi-room configuration.

5.4 Calibration

A calibration factor is proposed as a multiplier to the calculated thermal conductivity applicable to each non-char element where the temperature of that element is higher than 50 °C. This effectively corresponds to the pyrolysis region and a heated zone that extends deeper within the section. The multiplier is based on a simple trial and error procedure. The calibration process first involves isolating the pyrolysis model from the fire model and supplying defined boundary conditions to the pyrolysis model i.e. a time temperature curve or heat flux value along with the oxygen mass fraction, and then comparing the char depth (based on the 300 °C isotherm) with experiments where the boundary conditions are clearly defined. The pyrolysis and charring submodel is benchmarked against constant heat flux experiments by Pope et al. [44] and furnace experiments by König and Walleij [45] as described in [subsubsection 6.2.1](#) and [subsubsection 6.2.2](#). These experiments are used to inform the selection of a suitable calibration factor. Results are then given in [subsection 6.4](#) using the coupled fire and pyrolysis model for simulations of three full-scale fire experiments in CLT enclosures where the resulting gas phase enclosure temperatures and solid phase char depths are compared with and without calibration.

6. Benchmarking

6.1 General

Benchmarking of the model is presented as three parts. Firstly, examining the pyrolysis model in isolation by imposing known boundary conditions in the form of a constant heat flux (see [subsubsection 6.2.1](#)) or a defined gas time temperature curve (see [subsubsection 6.2.2](#)). Secondly, the underlying zone model capability of characterising the thermal

environment in a fully protected CLT enclosure is examined without a contribution from any exposed timber surfaces (see [subsection 6.3](#)). Thirdly the two models are coupled and then used to predict the thermal environment and extent of charring in an enclosure with known areas of mass timber exposed (see [subsection 6.4](#)).

6.2 Pyrolysis model - decoupled

6.2.1 Constant heat flux experiments by Pope et al.

As part of an investigation into the measurement errors associated with thermocouples inserted perpendicular to a thermal wave in a charring material, Pope et al. [44] carried out experiments using the cone calorimeter apparatus that exposed laminated bamboo blocks to a constant heat flux. The specimens had dimensions $120 \times 120 \times 100$ mm thick and the lamellae were bonded together with a phenol-formaldehyde resin. The density of the bamboo was given as 675 kg/m^3 and moisture content was found to be approximately 6.5–7%. The composition of the bamboo was assumed to be 71% cellulose, 12 % hemicellulose, 10 % lignin and 10% water [46]. The ambient temperature was 25 °C.

Simulations using the pyrolysis and charring submodel are made, where the ambient oxygen mass fraction is taken as 0.23, the convective heat transfer coefficient as $10 \text{ W/m}^2\text{K}$ and the heat of combustion as 17.5 kJ/kg . The flame heat flux was determined using [Equation 20](#) and it was further assumed that if there was a flame present on the surface of the timber (i.e. $\dot{q}_f > 0$) then there was no convective heat losses from the surface.

[Figure 6](#) was adapted from Pope et al. [44] and shows the measured depth of the 60°C (blue lines) and 300°C (orange lines) isotherms based on thermocouples installed from the side and from the back of the specimen. The plot has been overlaid with the predicted char depths versus time without calibration (the dashed lines) and with calibration factors of 1.6 and 1.9 applied to the wood thermal conductivity, as previously described. The uncalibrated simulations provide reasonable agreement in the first 20 minutes of the experiment but underpredict for longer times. The calibration factor of 1.6 provides a reasonable correction though may have still underpredicted the measured char depth if the experiment had continued beyond 60 minutes.

6.2.2 Furnace experiments by König and Walleij

Three experiments using a fire resistance test furnace were carried out by König and Walleij [45] to measure the depth of char in timber sections 95 mm deep. The timber species used was a spruce with a dry density of $420 - 430 \text{ kg/m}^3$ conditioned at 20 °C and 65% RH. For the present calculations, a wet density of 470 kg/m^3 and moisture content of 10% are used. The furnace thermal exposures represented a standard time temperature curve and two parametric curves that both included decay phases as shown in [Figure 7](#) from reference [45]. Oxygen concentration in the furnace was not recorded but it is assumed in the present analysis to be no more than 10% by mass for the heating phases returning to ambient level (23% by mass) for the decay phase. [Figure 8](#) shows the char depth versus time based on the thermocouple measurements and 300 °C isotherm measured by König and Walleij [45] for the standard fire resistance curves labelled SFE in [Figure 7](#). The char depths predicted from the pyrolysis and charring submodel are overlaid on the plot and show the uncalibrated pyrolysis and charring model gives good agreement for the first 40 minutes or so but thereafter the char rate decreases in comparison with the experimental

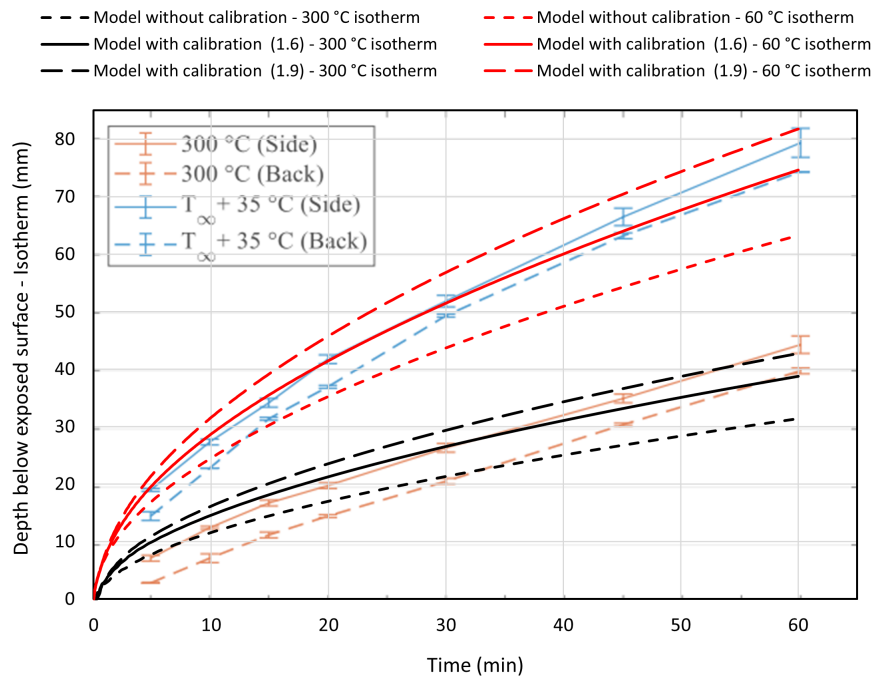


Figure 6. Laminated bamboo exposed to 60 kW/m² [44] with and without calibration.

values. The calibrated curve using a calibration factor of 1.6 provides more conservative predictions but the difference between the measured and predicted values is seen to reduce with time.

Figure 9 shows the char depth versus time based on the thermocouple measurements and 300 °C isotherm for the Test Series C1 to C3. This is the curve labelled 510/0,12 in Figure 7. The predicted char depths with and without calibration are overlaid on Figure 9. Again, the uncalibrated prediction shows good agreement only in the early period and underpredicts the ultimate char depth. While the prediction using a calibration factor of 1.6 provides good prediction of the ultimate char depth it tends to overpredict the char depth at earlier times. Figure 10 shows the char depth versus time for the second parametric curve labelled 170/0,04 in Figure 7. Again, the predicted char depths with and without calibration are overlaid on Figure 10 with similar trends shown, however the calibration factor of 1.6 produces an ultimate char depth that may still be considered too low.

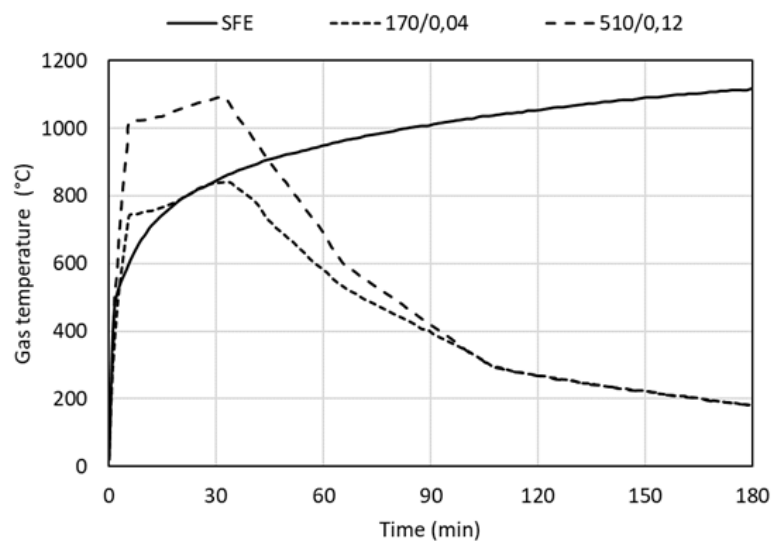


Figure 7. Furnace time-temperature histories for experiments (from König and Walleij [45]).

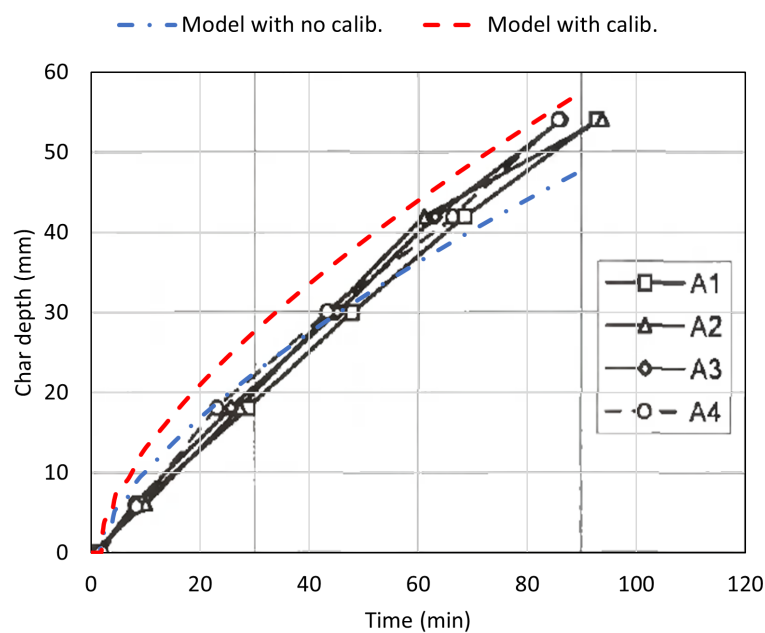


Figure 8. Depth of char due to standard fire resistance test exposure (König and Walleij [45] – SFE Test Series A) compared with model prediction.

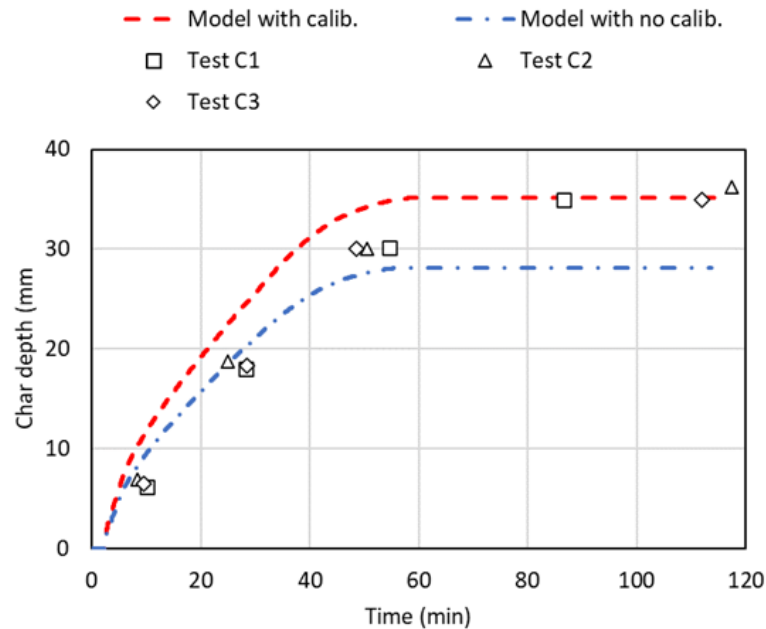


Figure 9. Depth of char due to standard fire resistance test exposure (König and Walleij [45] – Test Series C1 to C3) compared with model prediction.

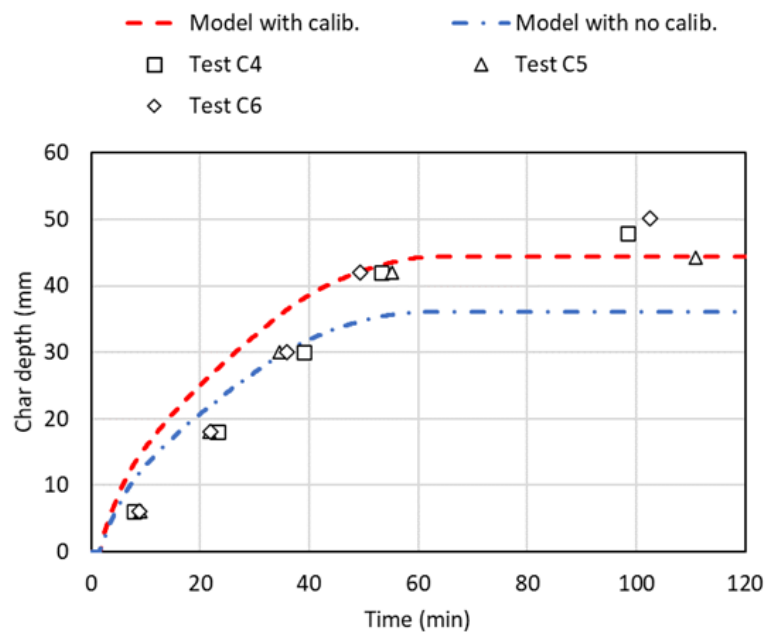


Figure 10. Depth of char due to standard fire resistance test exposure (König and Walleij [45] – Test Series C4 to C6) compared with model prediction.

6.3 Zone model - decoupled

This section describes four enclosure fire tests where the CLT was fully protected by gypsum plasterboard, to provide benchmarking cases for the zone model alone when decoupled from the pyrolysis model.

6.3.1 Carleton University room fire experiments

Two room experiments conducted at Carleton University were reported by Li et al. [47] where the room measured 4.5 m long \times 3.5 m wide \times 2.5 m high with a door opening 1.069 m wide \times 2.0 m high. The CLT walls were protected with two layers of 12.7 mm thick gypsum board. These were identical tests with no contribution from the CLT. The average HRR of Test 1 and 2 was reported, and due to system malfunction, only the gas temperature for Test 2 was reported [47]. All rooms were constructed from CLT panels manufactured by Nordic Engineered Wood [48]. They were 105 mm thick with nominal density 515 kg/m³ and comprised three layers each 35 mm thick. The layers were adhered with a polyurethane-based adhesive. The CLT floor panel in each room was protected with a layer of 15.9 mm (5/8 inch) thick Type X fire-rated gypsum board with a layer of 12.7 mm thick cement board installed on top. Over the cement board, a layer of 19 mm thick hardwood tongue and groove maple flooring was installed.

The thermal properties for the plasterboard linings were taken as: thermal conductivity 0.24 W/mK, specific heat 950 J/kg K and density 784 kg/m³ [49]. The fuel load was bedroom furniture and clothing and also included maple boards on the floor. Integrating the measured heat release rate curves from calorimetry, McGregor [50] estimated the actual energy release from the furniture for this case as 366 MJ/m². In these simulations, a heat of combustion for wood of 17.5 MJ/kg from Eurocode 5 [32] with an assumed combustion efficiency of 0.8 is used giving an effective value of 14 MJ/kg. The characteristic fuel thickness for the wood crib representation assumed in the simulations is 50 mm (and used in the mass loss rate equations for the wood crib). Since the CLT was fully protected it is assumed there is no contribution to the burning.

The postflashover model burning wood cribs allows an excess fuel factor to be included. For the case of the moveable fire load, a simulation with GER of 1.3 was used. GER of 1.3 means that, for ventilation control, the mass loss rate from the fuel will be 30% higher than can burn inside the room, and this is of the same order as noted previously for wood cribs burning in an enclosure.

Figure 11 and Figure 12 show the measured and predicted heat release rate and average upper layer gas temperature for these experiments. The rate of heat release is the sum of the energy generated inside the enclosure plus any combustion outside the room. The prediction is comparable to the average rate of heat release from oxygen calorimetry in the experiment. The gas temperature is also comparable to (with a slightly higher peak) the gas temperature history for the experiment.

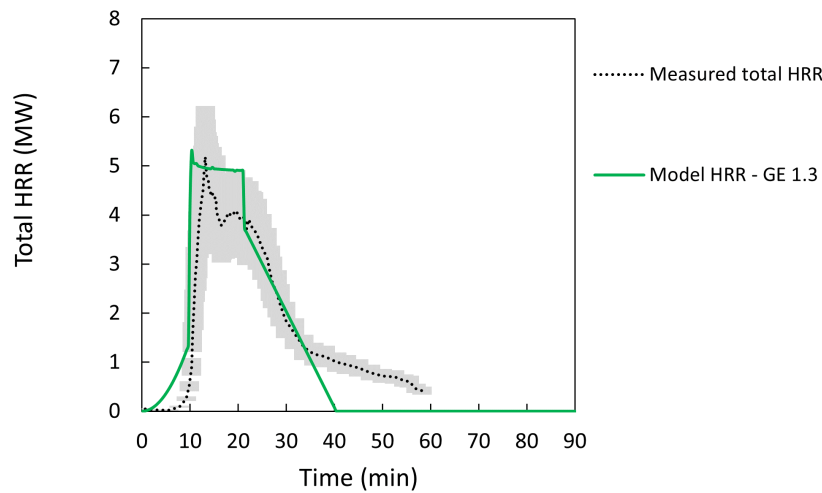


Figure 11. Measured and predicted total heat release rate for Carleton room fire experiments CLT fully protected with two layers of 12.7 mm thick gypsum board.

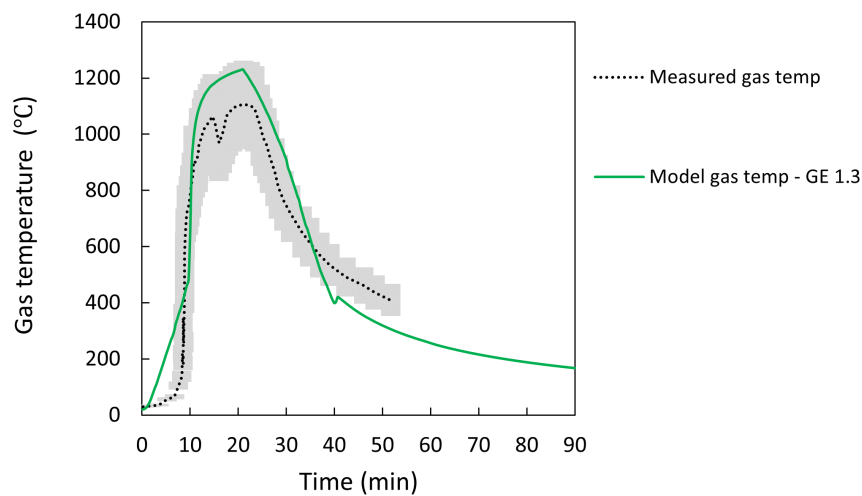


Figure 12. Measured and predicted enclosure gas temperatures for Carleton room fire experiments CLT fully protected with two layers of 12.7 mm thick gypsum board.

6.3.2 NFPA Research Foundation room fire experiments

For research done for the NFPA Research Foundation, Su et al. [51] conducted a series of full-scale enclosure experiments in a CLT enclosure with various amounts of exposed wall and ceiling areas. These enclosures were intended to represent a studio sized apartment unit. The CLT was 175 mm thick with five lamellae each 35 mm thick. The lamellae were adhered with a polyurethane adhesive that was not considered to be thermally resistant. The enclosure measured $9.1 \times 4.6 \times 2.7$ m high.

Two of these experiments are included here where all the CLT surfaces were fully protected with gypsum plasterboard. The only difference between the experiments was the

size of the opening located in one of the shorter walls. The two opening sizes considered were: 2.0 m high \times 1.8 m wide; and 2.0 m high \times 3.6 m wide. In addition to the main opening, there were two additional small openings in the opposite (rear) wall. Each one was 150 mm diameter and positioned 0.3 m and 1.8 m above the floor. These were intended to simulate leakage of gases through a protected entrance doorway.

The fuel load comprised mostly cellulosic furniture (white pine, hardboard and Douglas fir) with a small amount of polyurethane foam (about 3% by mass). Wade [5] estimated the fire load density to be 391 MJ/m² consistent with an average effective heat of combustion of 14 MJ/kg.

In Test 1-1, with an opening 1.8 m wide \times 2.0 m high in one wall, the walls and ceiling were fully protected with 3 layers of 15.9 mm Type X gypsum plasterboard. The t^2 growth rate coefficient used is 0.0037 kW/s² to approximately match the experimental time to reach 500°C (flashover). The experiment is modelled assuming both the walls and ceiling were 175 mm thick wood covering with 48 mm of gypsum plasterboard.

Once again assuming an excess fuel factor of 1.3, Figure 15 shows the measured and predicted total rate of heat release and Figure 16 shows the measured and predicted gas temperatures. In both cases the agreement between the model and the measured values is considered to be good.

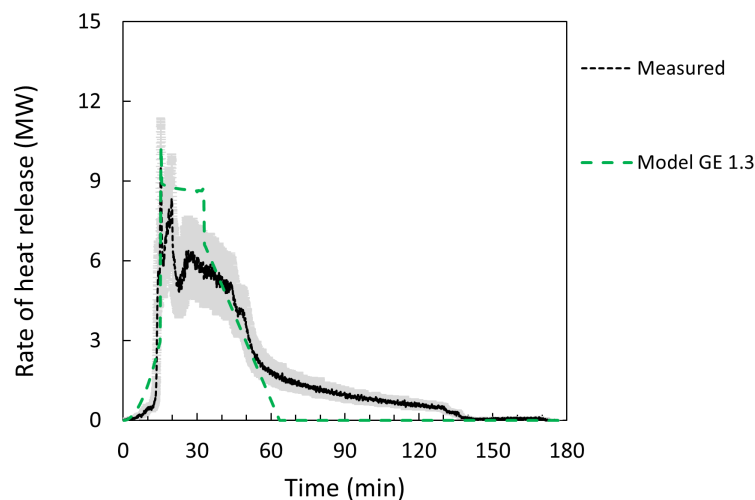


Figure 13. Measured and predicted total heat release rate for NFPA Research Foundation room fire Test 1-1 with CLT fully protected with three layers of 15.9 mm thick gypsum board.

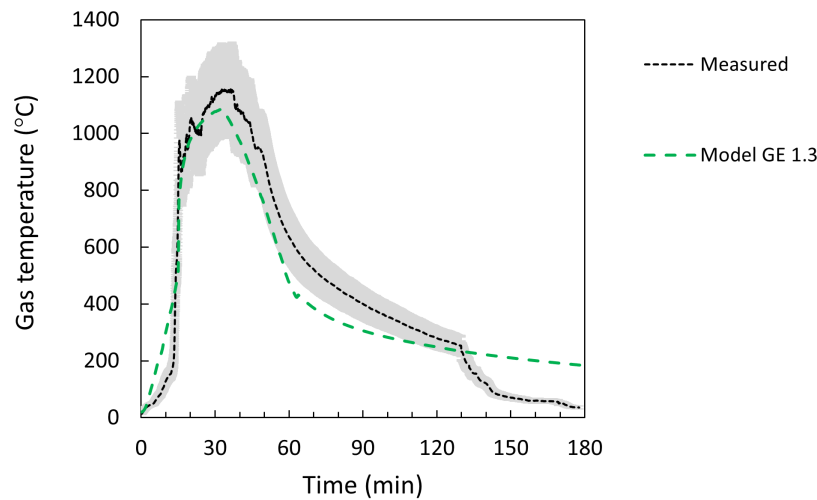


Figure 14. Measured and predicted total heat release rate for NFPA Research Foundation room fire Test 1-1 with CLT fully protected with three layers of 15.9 mm thick gypsum board.

The second test configuration was referred to as Test 1-2 by Su et al. [51]. There was an opening 3.6 m wide \times 2.0 m high. The walls and ceiling were fully protected with 2 layers of 15.9 mm Type X gypsum plasterboard. The t^2 growth rate coefficient used was 0.0052 kW/s² to approximately match the experimental time to reach 500°C (flashover). This test differed from Test 1-1 by having double the area of ventilation for the largest opening.

Flashover occurred at 15.3 min followed by a large external fire plume. The fire started to decay at 37 min and external flaming ceased from 40 min. The model prediction of the peak gas temperature is clearly lower than measured in this experiment as seen in Figure 16 unlike for Test 1-1 where a good prediction of the peak gas temperature is achieved. On the other hand, the prediction of the total rate of heat release appears in good agreement as seen in Figure 15. The model considered this experiment to be fuel surface area controlled and not ventilation limited as for Test 1-1 where a period of ventilation controlled burning of about 20 minutes duration is apparent from the plateau in the predicted rate of heat release curve (Figure 15). The poor agreement for the gas temperature might be interpreted as suggesting that the fuel surface controlled (free-burning) mass loss rate for the wood cribs was not a good representation of the real furniture used in this experiment.

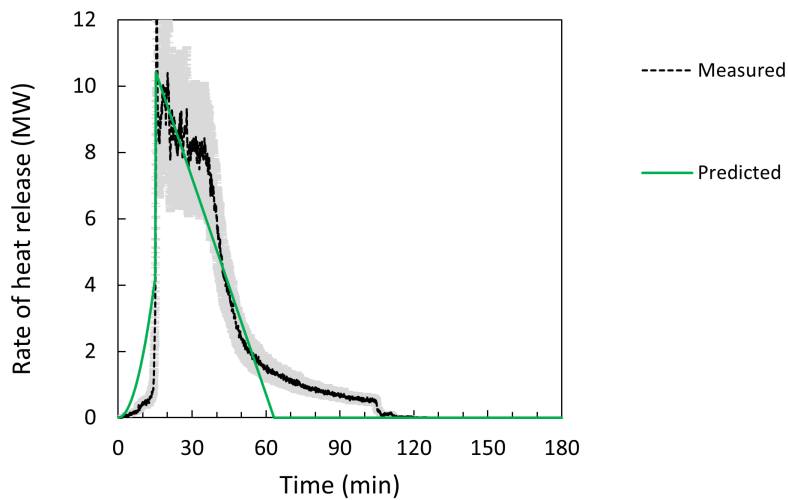


Figure 15. Measured and predicted total heat release rate for NFPA Research Foundation room fire Test 1-2 with CLT fully protected with two layers of 15.9 mm thick gypsum board.

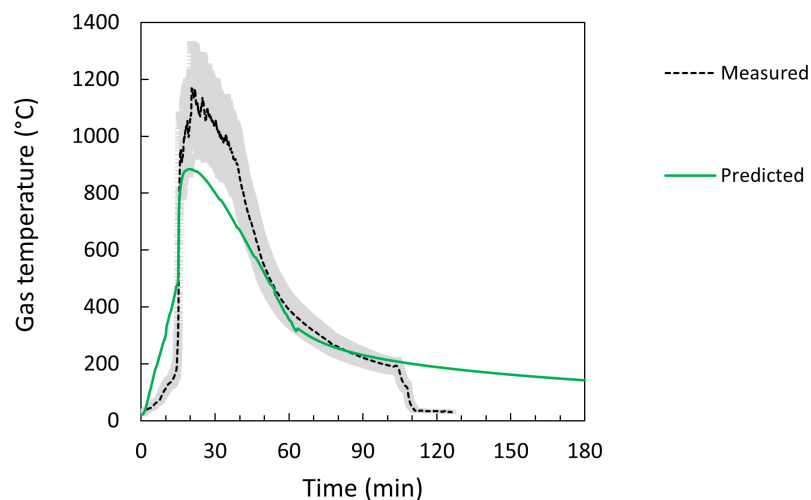


Figure 16. Measured and predicted total heat release rate for NFPA Research Foundation room fire test 1-2 with CLT fully protected with two layers of 15.9 mm thick gypsum board.

6.3.3 NRCC room fire experiments

An enclosure fire experiment with CLT panels and Glulam structural elements protected with 3 layers of Type X gypsum plasterboard (1/15.9 mm + 2/12.7 mm) were conducted at the National Research Council of Canada by Su et al. [52]. The enclosure was constructed from 175 mm thick CLT manufactured from spruce-pine-fir lumber using five lamellae each 35 mm thick and bonded together with a thermal resistive polyurethane adhesive which met the full-scale fire test requirements in ANSI/APA PRG-320-2018 [53]. The den-

sity of the CLT was not reported by Su et al. [52] but the same CLT specification was reported by Janssens [54] to have a nominal density of 505 kg/m^3 and similar to the nominal density of 515 kg/m^3 for the CLT used in experiments by McGregor [50]. The enclosure measured 4.5 m long \times 2.4 m wide \times 2.7 m high with a single doorway opening in one of the longer walls measuring 0.76 m wide \times 2.0 m high. The fuel contents in each experiment comprised three wood cribs each weighing 120 kg . The wood cribs were constructed from 0.9 m long sticks of $95 \times 38 \text{ mm}$ spruce.

Based on the mass of wood cribs (360 kg) and an assumed effective heat of combustion of 14 MJ/kg [32], it is determined that the fire load energy density for the moveable fire load is 467 MJ/m^2 . The initial fire growth is assumed to be a Fast t^2 fire until flashover after which the mass loss rate of the moveable fire load is determined from the lesser of the ventilation-controlled burning rate, crib porosity-controlled burning rate and the fuel-controlled burning rate for wood cribs.

This experiment was designated Experiment 1 by Su et al. [52] and did not include any wood surface contribution. The average gas temperature shown in Figure 17 is the average temperature reading from the thermocouple trees inside the enclosure. The shaded region shown corresponds to the range of temperatures measured by individual thermocouples on the thermocouple trees. Figure 17 also shows the gas temperature measured in the doorway opening at heights of 0.6 , 1.2 and 1.6 m above the floor. The peak average gas temperature in the room of 1129°C was measured at about 19 min . The gas temperature predicted by the fire model (peak 1146°C at 21 min) provides good agreement with the measured average gas temperature from the thermocouple trees until the latter part of the decay where the predicted temperatures are higher than those measured. This change in slope in the predicted temperature occurs following predicted burnout of the contents and is due to the 'hot' layer ceasing to vent once the layer interface in the enclosure lifted to reach the top of the opening.

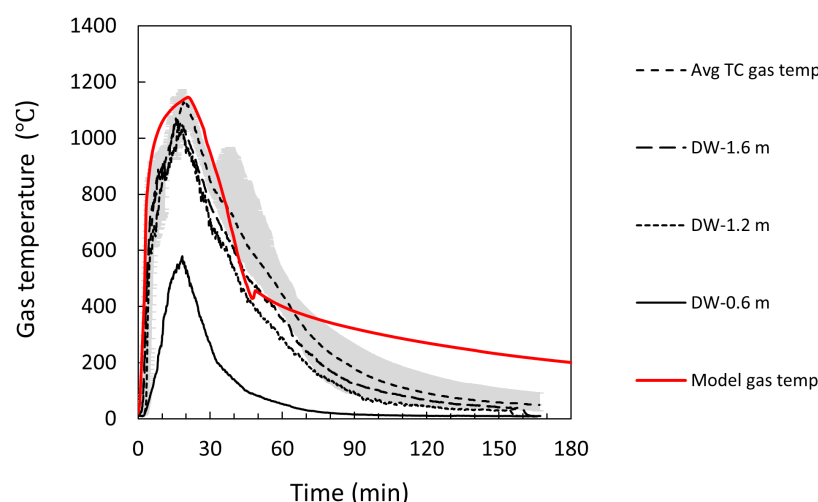


Figure 17. Measured and predicted gas temperatures for room fire experiment 1 with CLT fully protected with three layers of gypsum board.

6.4 Zone and pyrolysis model - coupled

6.4.1 NRCC room fire experiments

Su et al. [52] at the National Research Council of Canada conducted five full-scale fire experiments burning wood cribs within a CLT enclosure with an opening. The CLT was 175 mm thick CLT manufactured using five lamellae, each 35 mm thick and bonded together with a thermal resistive polyurethane adhesive. The enclosure measured 4.5 m long \times 2.4 m wide \times 2.7 m high with a single doorway opening in one of the longer walls measuring 0.76 m wide \times 2.0 m high. The fuel contents in each experiment comprised three wood cribs each weighing 120 kg providing a nominal fire load of 467 MJ/m² (assuming an effective heat of combustion of 14 MJ/kg). Encapsulation was provided, where required, by 2–3 layers of 15.9 mm thick Type X gypsum board. Two of the experiments are considered here which only involved areas of exposed wall and ceiling. Experiment 2 had 33% of the wall and 10% of the ceiling area exposed (or unprotected) and Experiment 5 had 35% of the wall and 100% of the ceiling exposed.

Figure 18 shows the gas temperature versus time measured inside the enclosure and in the doorway for Experiment 2. The maximum char depths measured in the upper wall ranged from 50 – 70 mm (mean 55.6 mm) and the maximum char depth in the ceiling ranged from 45 – 63 mm (mean 52.5 mm). Figure 18 also shows the predicted gas temperature from the coupled fire and pyrolysis submodels with several different calibration factors used as well as with no calibration (i.e. $k = 1.0$).

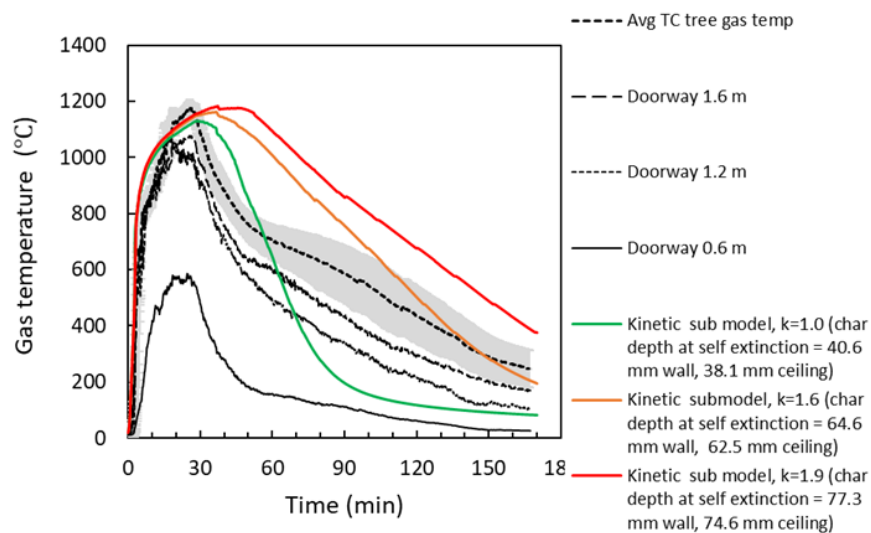


Figure 18. Enclosure Experiment 2 (33% walls and 10% ceiling exposed).

Figure 19 shows the corresponding graph for Experiment 5. The maximum char depths measured in the upper wall ranged from 81 – 109 mm (mean 88.6 mm) and the maximum char depth in the ceiling ranged from 70 – 90 mm (mean 77.5 mm).

6.4.2 NFPA Research Foundation room fire experiments

Su et al. [51] conducted a series of full-scale enclosure experiments in a CLT enclosure with various amounts of exposed wall and ceiling areas. The CLT was 175 mm thick with five lamellae each 35 mm thick. The lamellae were adhered with a polyurethane adhesive.

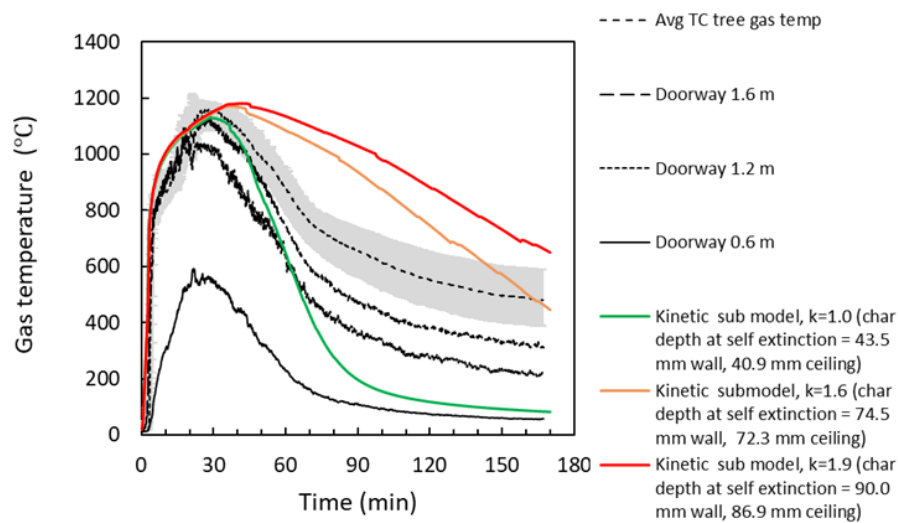


Figure 19. Enclosure Experiment 5 (35% walls and 100% ceiling exposed).

One of these experiments is included here – referred to as Test 1-4. The enclosure measured $9.1 \times 4.6 \times 2.7$ m high with an opening 2.0 m high and 1.8 m wide. The ceiling was fully exposed with all walls protected with gypsum plasterboard. Figure 20 shows the gas temperature versus time measured inside the enclosure. The increase in gas temperature after 120 minutes is due to delamination of CLT that allowed the fire to grow again upon exposing fresh fuel. For the current analysis, delamination is ignored on the assumption that it can be avoided by using a thermally resistive adhesive to bond the CLT lamellae together or through improved consideration of the CLT lay-up, e.g. increasing the thickness of the room facing lamellae. Brandon [55] conducted additional intermediate scale experiments and estimated the char depth for this experiment as 50 mm in the absence of any delamination.

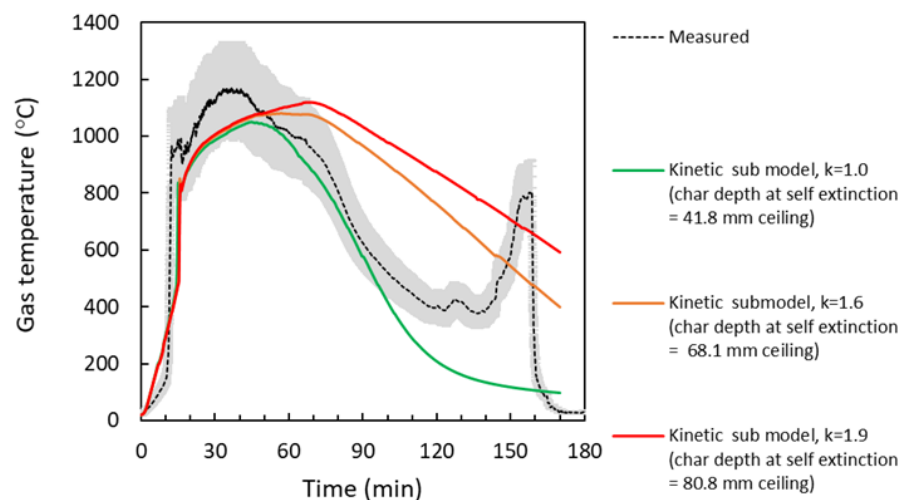


Figure 20. Enclosure Test 1-4 (100% ceiling only exposed).

6.5 Char depth validation

Six compartment fire experiments were selected to provide validation for the char depth predictions using compartment fire experiments where:

1. the contents fuel was furniture or wood cribs;
2. the exposed wood surfaces were principally on one surface or where reradiation between surfaces was small; and
3. there was no significant char falloff (ie delamination or debonding of lamella) during the fire;
4. the experimental char depth had previously been determined or estimated at the end of the experiment.

The experimental parameters and measured char depths for each experiment are taken from summary data provided by Brandon [2] (and previously used to validate the engineering method proposed by Brandon) and also from Wade [5].

The fire experiments are summarised in Table 3. Experiments 1 and 2 were conducted by Su et al. [51]; Experiments 3 and 4 by Zelinka et al. [56]; Experiment 5 by Medina Hevia [57] and Experiment 6 by Su et al. [52].

Brandon [2] previously proposed an engineering method based on the parametric fire equations in conjunction with an iterative procedure to estimate the char depth in an enclosure with exposed mass timber by adjusting the fuel density at each iteration. The method is not described here (see [2]) but the predictions are also included in Table 3 for comparison.

A plot of predicted versus experimentally determined char depth for the B-RISK kinetic submodel, B-RISK simple GE submodel and the calculated char depth using Brandon's method is shown in Figure 21. The B-RISK model predictions have conservatively assumed all the pyrolysed fuel is burned in the enclosure (i.e. GER = 1) with nominal char temperatures of 270 °C and 300 °C as shown.

Table 3. Summary of key experimental parameters and model char depth predictions.

Experiment	Test ID & Ref.	Dimensions (m)	Opening size (width x height m)	Unprotected area	Movable fire load per floor area (MJ/m ²)	Char depth from experiment (mm)	Calc. char depth using Brandon's method (mm)	Calc. char depth using kinetic submodel (mm) *	Calc. char depth using simple GE submodel (mm) *
1	1-3 [51]	4.6 x 9.1 x 2.7	3.6 x 2	33% of walls	550	35	45	41	39
2	1-4 [51]	4.6 x 9.1 x 2.7	3.6 x 2	100% of ceiling	550	40	79	54	70
3	A2 [56]	9.1 x 9.1 x 2.7	3.66 x 2.44 (x 2 openings)	18% of ceiling	550	23	49	45	36
4	A3 [56]	9.1 x 9.1 x 2.7	3.66 x 2.44 (x 2 openings)	30% of walls	550	23	32	38	37
5	K3 [57]	3.5 x 4.5 x 2.5	1.1 x 2	30% of walls	532	44	46	41	44
6	2 [52]	4.5 x 2.4 x 2.7	0.76 x 2	10% of ceiling, 33% of walls	550	68	67	72	64

* char temp 270 C

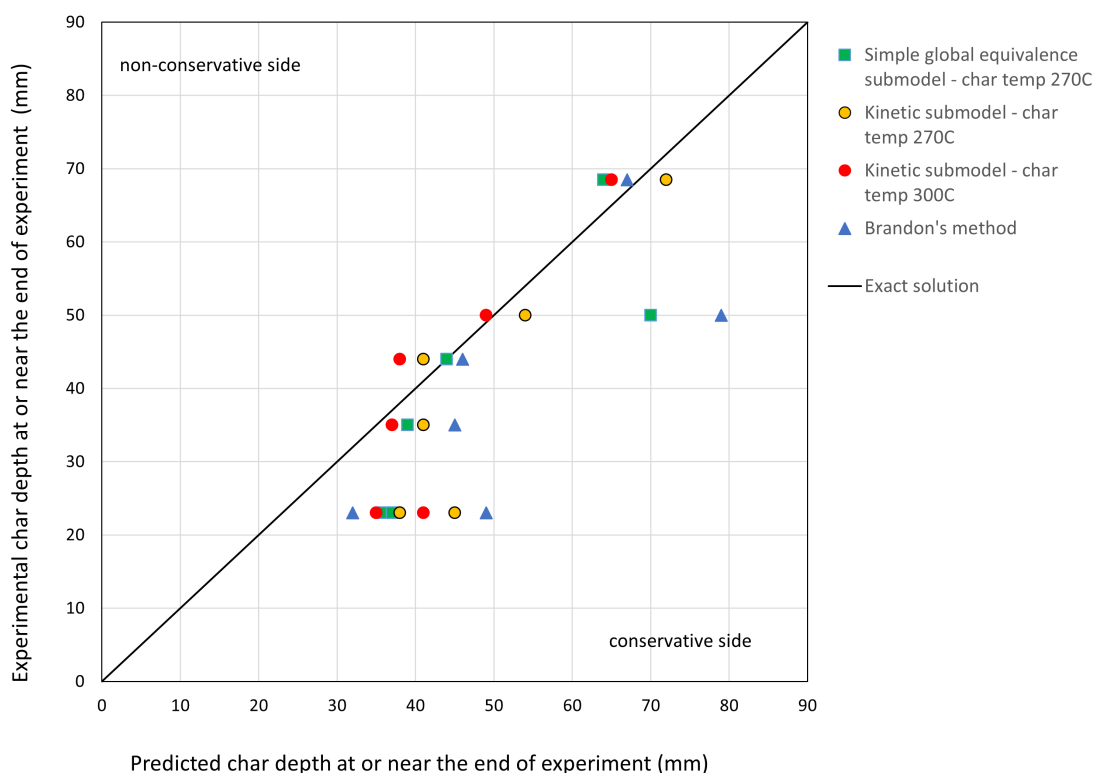


Figure 21. Predicted versus experimentally determined char depth for the kinetic submodel, simple GE submodel and also including calculations using Brandon's method.

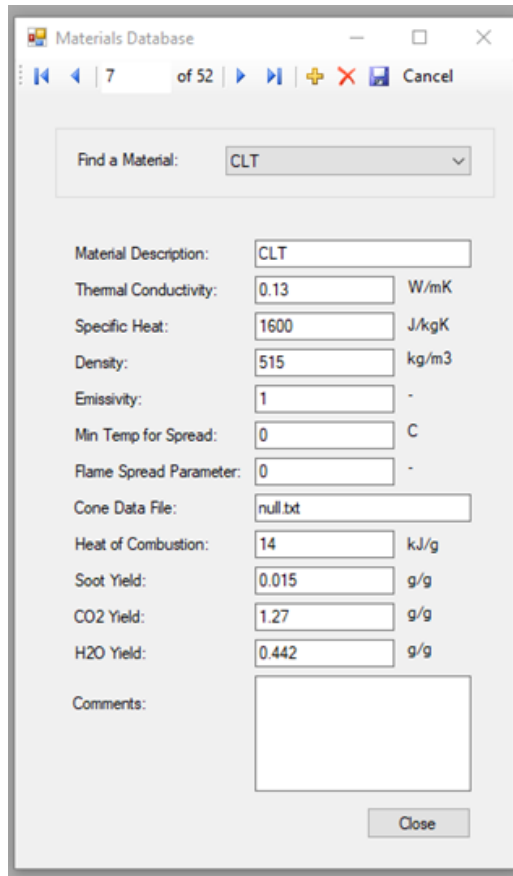
All three methods give reasonable and mostly conservative predictions of the char depth. More conservative B-RISK predictions can be ensured by using a slightly lower assumed char temperature, and by assuming all combustion takes place within the enclosure.

7. User guide

7.1 Instructions for the mass timber kinetic pyrolysis submodel

This section describes how to set up and use the kinetic submodel for a fire in an exposed mass timber compartment.

1. The thermal properties database should contain a material corresponding to the mass timber, for example that shown in [Figure 22](#). The values for thermal conductivity and specific heat will be overridden by the calculations described in [subsection 4.4](#) and [subsection 4.5](#), with the remaining inputs used as entered here.



Materials Database

Find a Material: CLT

Material Description: CLT

Thermal Conductivity: 0.13 W/mK

Specific Heat: 1600 J/kgK

Density: 515 kg/m³

Emissivity: 1 -

Min Temp for Spread: 0 C

Flame Spread Parameter: 0 -

Cone Data File: null.txt

Heat of Combustion: 14 kJ/g

Soot Yield: 0.015 g/g

CO₂ Yield: 1.27 g/g

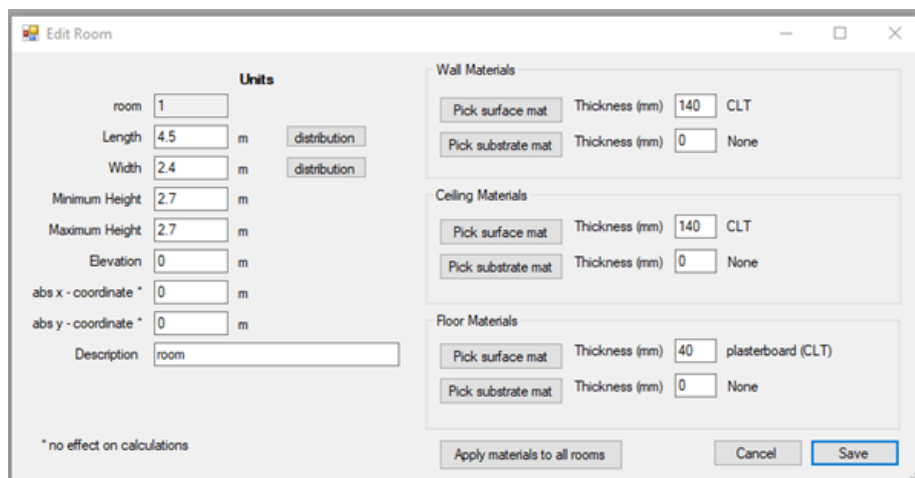
H₂O Yield: 0.442 g/g

Comments:

Close

Figure 22. Example entry for a CLT material in the thermal database.

- The material should be added to the wall and ceiling of the compartment as shown in [Figure 23](#) along with the relevant dimensions for the enclosure. Note that the overall thickness of the CLT should be an exact multiple of the CLT lamella thickness, and no substrate material should be specified.



Edit Room

Units

room: 1

Length: 4.5 m

Width: 2.4 m

Minimum Height: 2.7 m

Maximum Height: 2.7 m

Elevation: 0 m

abs x - coordinate: 0 m

abs y - coordinate: 0 m

Description: room

* no effect on calculations

Wall Materials

Pick surface mat: Thickness (mm) 140 CLT

Pick substrate mat: Thickness (mm) 0 None

Ceiling Materials

Pick surface mat: Thickness (mm) 140 CLT

Pick substrate mat: Thickness (mm) 0 None

Floor Materials

Pick surface mat: Thickness (mm) 40 plasterboard (CLT)

Pick substrate mat: Thickness (mm) 0 None

Apply materials to all rooms

Cancel

Save

Figure 23. Room input parameters.

- The relevant parameters for the mass timber pyrolysis model are entered from the

Room Design, Mass Timber (CLT) menu item shown in shown in Figure 24 and with the input form shown in Figure 25.

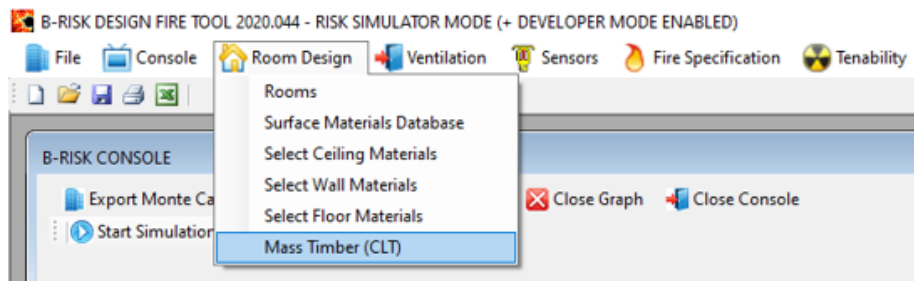
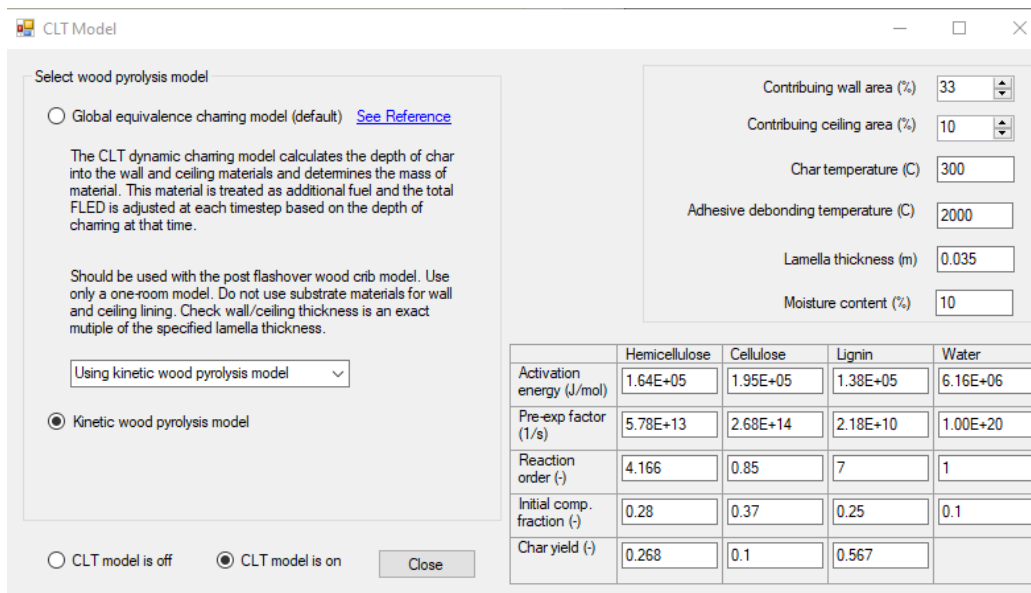


Figure 24. Menu selection for the mass timber pyrolysis model.



Select wood pyrolysis model

☐ Global equivalence charring model (default) [See Reference](#)

The CLT dynamic charring model calculates the depth of char into the wall and ceiling materials and determines the mass of material. This material is treated as additional fuel and the total FLED is adjusted at each timestep based on the depth of charring at that time.

Should be used with the post flashover wood crib model. Use only a one-room model. Do not use substrate materials for wall and ceiling lining. Check wall/ceiling thickness is an exact multiple of the specified lamella thickness.

Using kinetic wood pyrolysis model

☒ Kinetic wood pyrolysis model

☐ CLT model is off ☒ CLT model is on

Contributing wall area (%) 33

Contributing ceiling area (%) 10

Char temperature (C) 300

Adhesive debonding temperature (C) 2000

Lamella thickness (m) 0.035

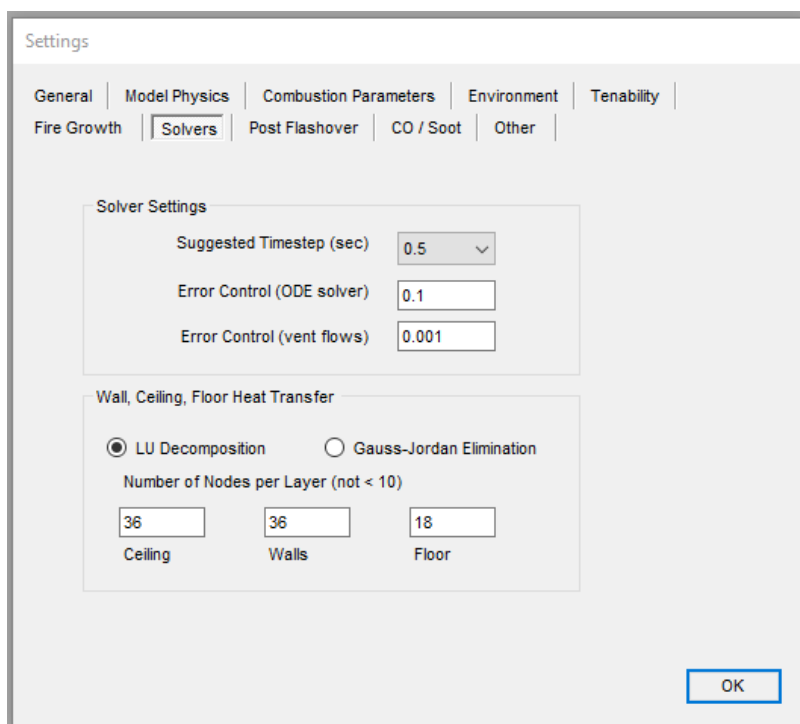
Moisture content (%) 10

	Hemicellulose	Cellulose	Lignin	Water
Activation energy (J/mol)	1.64E+05	1.95E+05	1.38E+05	6.16E+06
Pre-exp factor (1/s)	5.78E+13	2.68E+14	2.18E+10	1.00E+20
Reaction order (-)	4.166	0.85	7	1
Initial comp. fraction (-)	0.28	0.37	0.25	0.1
Char yield (-)	0.268	0.1	0.567	

Figure 25. Parameters for the mass timber pyrolysis model.

- As shown in Figure 25, to use the mass timber pyrolysis model the **CLT model is on** radio button option should be selected along with the **Kinetic wood pyrolysis model** radio button option.
- The percentage of wall and ceiling area comprising exposed mass timber should be entered. The char temperature can be specified. For this submodel, it is recommended that a char temperature of 270 °C be used instead of 300 °C for added conservatism.
- The lamella thickness should be entered. It must be exactly divisible into the overall specified wall thickness. In this example for a 140 mm thick wall or ceiling element there will be four lamella each 0.035 m thick.
- The moisture content as a percentage by mass is entered.

8. The kinetic properties shown in the table on the form can be used with the initial component fractions adjusted as requested to suit the specified mass fraction of water. The sum of the component fraction should be 1. It is recommended that the default kinetic property set be used.
9. The solver settings are reached using the **Misc Settings, Solvers** menu item with the form shown in Figure 26. It is recommended that the number of nodes per layer for the wall and ceiling be set such that the finite element thickness is 1 mm. In the example shown for a 140 mm thick wall with each lamella 35 mm thick, the number of nodes for each lamella is then 36.



Settings

General | Model Physics | Combustion Parameters | Environment | Tenability |
Fire Growth | **Solvers** | Post Flashover | CO / Soot | Other

Solver Settings

Suggested Timestep (sec) 0.5

Error Control (ODE solver) 0.1

Error Control (vent flows) 0.001

Wall, Ceiling, Floor Heat Transfer

☒ LU Decomposition ☐ Gauss-Jordan Elimination

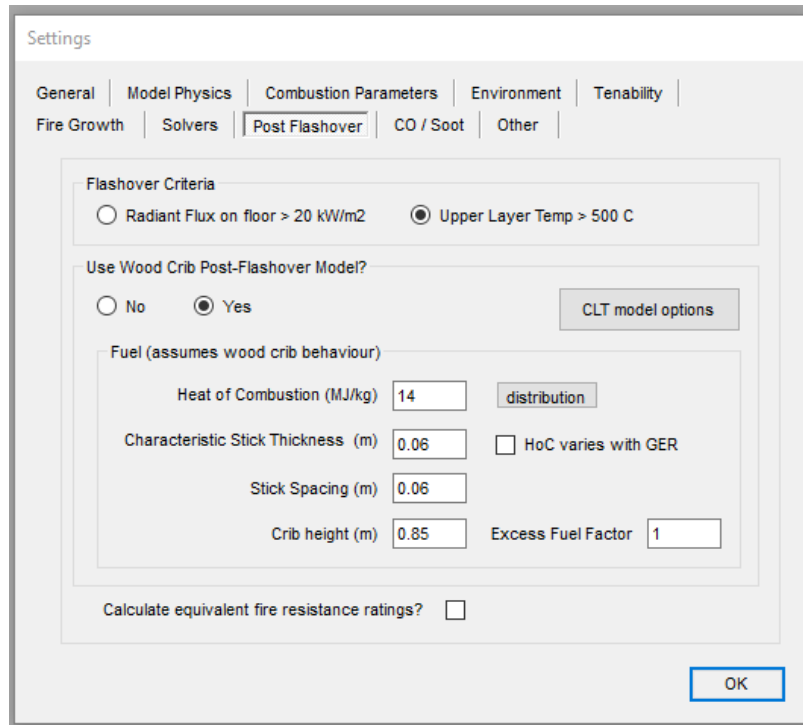
Number of Nodes per Layer (not < 10)

36 36 18
Ceiling Walls Floor

OK

Figure 26. Solver settings for the mass timber pyrolysis model.

10. The mass timber pyrolysis model is used in conjunction with the postflashover sub-model with the settings reached from the **Misc Settings, Postflashover Behaviour** menu item as shown in Figure 27. The option for **Use Wood Crib Postflashover Model** should be set to **yes**. To ensure a more conservative prediction, it is suggested that the Excess Fuel Factor be set equal to 1. This will mean all the fuel will burn inside the room with no external burning.



Settings

General | Model Physics | Combustion Parameters | Environment | Tenability |
Fire Growth | Solvers | **Post Flashover** | CO / Soot | Other

Flashover Criteria
☐ Radiant Flux on floor > 20 kW/m2 ☒ Upper Layer Temp > 500 C

Use Wood Crib Post-Flashover Model?
☐ No ☒ Yes CLT model options

Fuel (assumes wood crib behaviour)

Heat of Combustion (MJ/kg)	<input type="text" value="14"/>	distribution
Characteristic Stick Thickness (m)	<input type="text" value="0.06"/>	<input type="checkbox"/> HoC varies with GER
Stick Spacing (m)	<input type="text" value="0.06"/>	
Crib height (m)	<input type="text" value="0.85"/>	Excess Fuel Factor <input type="text" value="1"/>

Calculate equivalent fire resistance ratings? ☐

OK

Figure 27. Post flashover settings for the mass timber pyrolysis model.

11. Once the model is set up and the preceding parameters for the pyrolysis model have been set, the model is run as usual using the **Start Simulation** menu item.
12. Output from the model for the char depth can be obtained from the **Single Run Graphs, Surface Internal Temperatures, Wall - char depth** menu item as shown in [Figure 28](#) and [Figure 29](#).

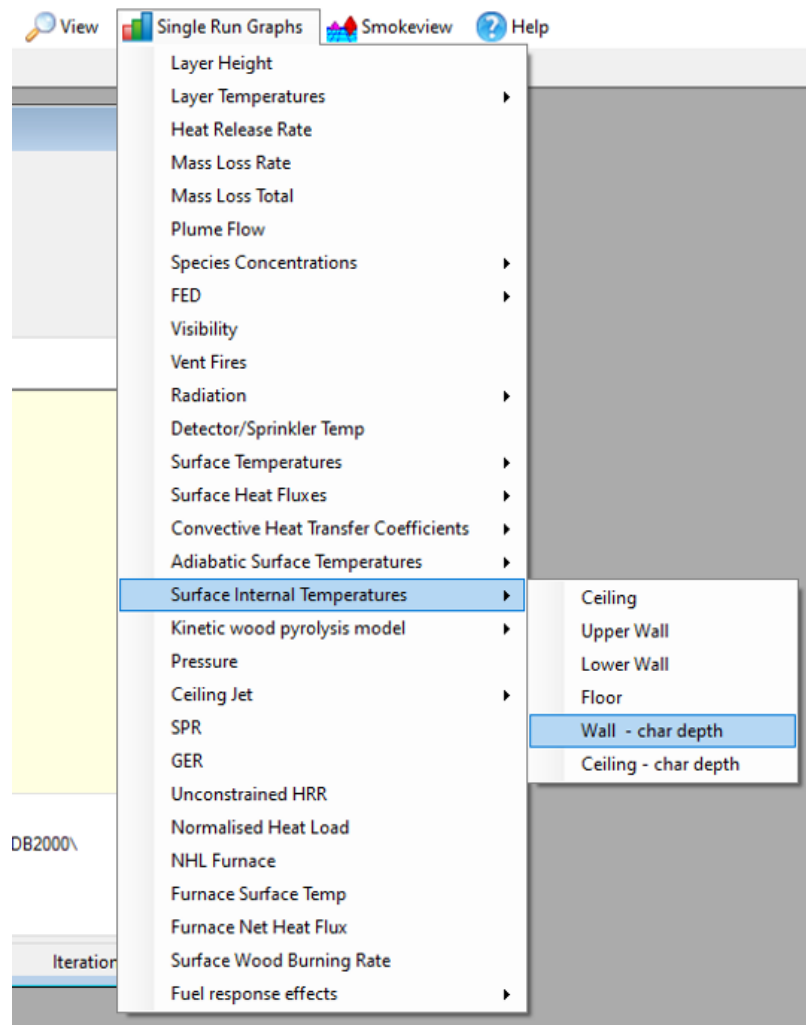


Figure 28. Menu item to view graph of char depth output.

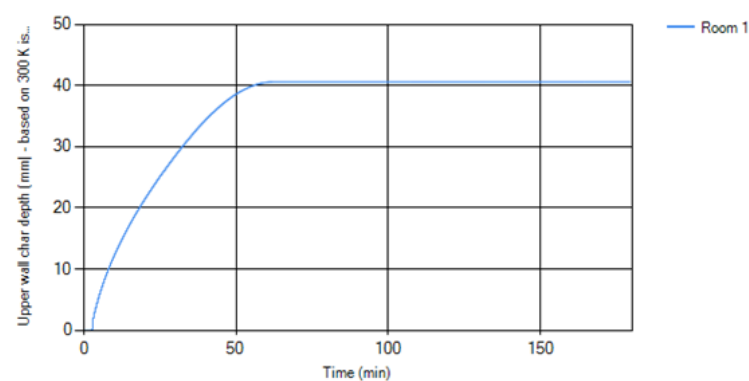


Figure 29. Graph of char depth output.

7.2 Calibration factor for the mass timber kinetic pyrolysis submodel

A calibration factor acting as a multiplier to the calculated thermal conductivity on the non-char elements above 50 °C, as discussed in [subsection 5.4](#) and [section 6](#), is set at 1.6 as a default value. This can be changed by the user, if required, from the File, Utilities, Kinetic Model Testing menu item as shown in [Figure 30](#).

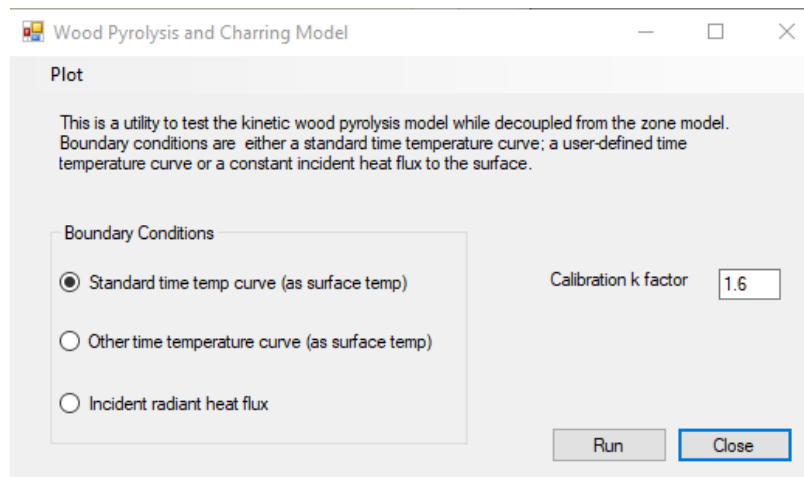


Figure 30. Changing the kinetic pyrolysis calibration factor.

References

[Citing pages are listed after each reference.]

- [1] D. Barber, R. Crielaard, and X. Li. Towards fire safety design of exposed timber in tall timber buildings. In *Proceedings of WCTE 2016 World Conference on Timber Engineering*, Vienna Austria, 2016. [Page 1.]
- [2] D. Brandon. Fire safety challenges of tall wood buildings – Phase 2: Task 4 Engineering methods. Report FRPF-2018-04, Fire Protection Research Foundation, Quincy, MA, 2018. [Pages 1 and 32.]
- [3] C.A. Wade, M.J. Spearpoint, C.M. Fleischmann, G.B. Baker, and A.K. Abu. Predicting the fire dynamics of exposed timber surfaces in compartments using a two-zone model. *Fire Technology*, 54(4):893–920, 2018. ISSN 0015-2684. doi: 10.1007/s10694-018-0714-2. [Page 1.]
- [4] C.A. Wade, D. Hopkin, J. Su, M.J. Spearpoint, and C.M. Fleischmann. Enclosure fire model for mass timber construction - benchmarking with a kinetic pyrolysis sub-model. In *Interflam 2019: 15th International Conference on Fire Science and Engineering*, Royal Holloway College, Nr Windsor, UK, 2019. InterScience Communications Limited. [Page 1.]
- [5] C. A. Wade. *A theoretical model of fully developed fire in mass timber enclosures*. PhD Thesis, University of Canterbury, Department of Civil and Natural Resources Engineering, Christchurch, New Zealand, 2019. [Pages 1, 17, 26, 32, and 56.]
- [6] C.A. Wade, D.J. Hopkin, M.J. Spearpoint, and C.M. Fleischmann. Calibration of a Coupled Post-flashover Fire and Pyrolysis Model for Determining Char Depth in Mass Timber Enclosures. In *Structures in Fire Proceedings of the Eleventh International Conference*, Brisbane, Australia, 2020. [Page 1.]
- [7] C.A. Wade, G.B. Baker, K. Frank, R Harrison, and M.J. Spearpoint. B-RISK 2016 User guide and technical manual. Study Report SR364, BRANZ, Porirua, New Zealand, 2016. [Page 1.]
- [8] R.D. Peacock, W.W. Jones, P.A. Reneke, and G.P. Forney. CFAST – Consolidated Model of Fire Growth and Smoke Transport (Version 6) User’s Guide. NIST Special Publication 1019 Sixth Edition 1041, National Institute of Standards and Technology, Washington, DC, 2005. [Page 1.]
- [9] L.Y. Cooper and G.P. Forney. The Consolidated Compartment Fire Model (CCFM) Computer Code Application CCFM.VENTS – Part III: Catalog of Algorithms and Subroutines. NISTIR 4344, National Institute of Standards and Technology, Gaithersburg, MD, 1990. [Page 2.]
- [10] L.Y. Cooper and G.P. Forney. The Consolidated Compartment Fire Model (CCFM) Computer Code Application CCFM.VENTS – Part I: Physical Basis. NISTIR 4342, National Institute of Standards and Technology, Gaithersburg, MD, 1990. [Page 2.]
- [11] Y. Utiskul. *Theoretical and experimental study on fully developed compartment fires*. PhD, University of Maryland, College Park, MD, 2007. [Pages 2 and 48.]

- [12] ISO. ISO 16734 Fire safety engineering – Requirements governing algebraic equations – Fire plumes. International Standard, International Organization for Standardization, Geneva, Switzerland, 2006. [Page 2.]
- [13] B.J. McCaffrey. Momentum implications for buoyant diffusion flames. *Combustion and Flame*, 52:149–167, 1983. doi: 10.1016/0010-2180(83)90129-3. [Pages 2, 47, and 49.]
- [14] G.P. Forney. Computing radiative heat transfer occurring in a zone fire model. NISTIR 4709, National Institute of Standards and Technology, Gaithersburg, MD, 1991. [Page 2.]
- [15] Appendix 3: Fuel properties and combustion data. Table A39. In M.J. Hurley, editor, *SFPE Handbook of Fire Protection Engineering*, page 3468. Springer, New York, NY, fifth edition edition, 2016. ISBN 978-1-4939-2564-3. [Page 2.]
- [16] A. Tewarson, F.H. Jiang, and T. Morikawa. Ventilation Controlled Combustion of Polymers. *Combustion and Flame*, 95(1-2):151–169, 1993. doi: 10.1016/0010-2180(93)90058-B. [Page 2.]
- [17] P.H. Thomas. Testing products and materials for their contribution to flashover in rooms. *Fire and Materials*, 5(3):103–111, 1981. ISSN 1099-1018. doi: 10.1002/fam.810050305. [Page 3.]
- [18] V. Babrauskas. Heat release rates. In M.J. Hurley, editor, *SFPE Handbook of Fire Protection Engineering*. Springer, New York, NY, 5th edition edition, 2016. ISBN 978-1-4939-2565-0. URL https://doi.org/10.1007/978-1-4939-2565-0_26. [Pages 3 and 4.]
- [19] C. Huggett. Estimation of rate of heat release by means of oxygen consumption measurements. *Fire and Materials*, 4:61–65, 1980. doi: 10.1002/fam.810040202. [Pages 3 and 48.]
- [20] W.M. Pitts. The Global Equivalence Ratio Concept and the Prediction of Carbon Monoxide Formation in Enclosure Fires. NIST Monograph 179, National Institute of Standards and Technology, June 1994. [Page 3.]
- [21] F.P. Incropera and D.P. DeWitt. *Fundamentals of heat and mass transfer*. John Wiley and Sons, NJ, USA, 1990. ISBN 978-0-471-30460-9. [Pages 5 and 6.]
- [22] A. Bartlett, R. Hadden, and L. Bisby. A Review of Factors Affecting the Burning Behaviour of Wood for Application to Tall Timber Construction. *Fire Technology*, November 2018. doi: 10.1007/s10694-018-0787-y. [Page 7.]
- [23] U. Wickström, D. Duthinh, and K. McGrattan. Adiabatic surface temperature for calculating heat transfer to fire exposed structures. In *Proceedings of the 11th International Conference on Fire Science & Engineering (INTERFLAM)*, Royal Holloway College, Nr Windsor, UK, 2007. InterScience Communications Limited. [Page 7.]
- [24] D.J. Rasbash, D.D. Drysdale, and D. Deepak. Critical heat and mass transfer at pilot ignition and extinction of a material. *Fire Safety Journal*, 10(1):1–10, January 1986. ISSN 0379-7112. doi: 10.1016/0379-7112(86)90026-3. URL <http://www.sciencedirect.com/science/article/pii/0379711286900263>. [Pages 8 and 9.]
- [25] R.D. Peacock, G.P. Forney, P.A. Reneke, R. Portier, and W.W. Jones. CFAST, the Consolidated Model of Fire and Smoke Transport. NIST Technical Note 1299, National Institute of Standards and Technology, February 1993. [Pages 9 and 48.]

- [26] Alastair I. Bartlett. *Auto-extinction of engineered timber*. PhD Thesis, The University of Edinburgh, Edinburgh, Scotland, 2018. [Page 9.]
- [27] P.S. Veloo and J.G. Quintiere. Convective heat transfer coefficient in compartment fires. *Journal of Fire Sciences*, 31(5):410–423, 2013. doi: 10.1177/0734904113479001. [Page 9.]
- [28] Arne Inghelbrecht. *Evaluation of the burning behaviour of wood products in the context of structural fire design*. International Master of Science in Fire Safety Engineering, The University of Queensland and Ghent University, 2014. [Page 9.]
- [29] Carmen Gorska, Juan P. Hidalgo, and Jose L. Torero. Fire dynamics in mass timber compartments. *Fire Safety Journal*, page 103098, May 2020. ISSN 0379-7112. doi: 10.1016/j.firesaf.2020.103098. URL <http://www.sciencedirect.com/science/article/pii/S0379711220301338>. [Page 9.]
- [30] H.C. Tran. Experimental data on wood materials. In V. Babrauskas and S.J. Grayson, editors, *Heat Release in Fires*, pages 357–372. Elsevier Applied Science, Essex, England, 1992. ISBN 978-0-419-16100-4. [Page 10.]
- [31] M.J. Spearpoint. Predicting the ignition and burning rate of wood in the cone calorimeter using an integral model. NIST GCR 99-775, National Institute of Standards and Technology, Gaithersburg, MD, 1999. [Page 10.]
- [32] CEN. EN 1995 Eurocode 5 Design of timber structures Part 1-1: General - Common rules and rules for buildings. European Standard, European Committee for Standardization, Brussels, 2004. [Pages 10, 24, and 29.]
- [33] Forest Products Laboratory. *Wood Handbook - Wood as an Engineering Material*. General Technical Report FPL-GTR-190, Department of Agriculture, Forest Service, Forest Products Laboratory, Madison, Wisconsin, 2010. [Page 10.]
- [34] M.L. Janssens and B. Douglas. Wood and wood products. In C.A. Harper, editor, *Handbook of building materials for fire protection*. McGraw-Hill, 2004. ISBN 978-0-07-138891-7. [Pages 10, 11, 13, 14, 15, 17, and 18.]
- [35] M.L. Janssens. Thermo-physical properties for wood pyrolysis models. In *Proceedings of the Pacific Timber Engineering Conference*, pages 607–618, Gold Coast, Australia, 1994. [Page 11.]
- [36] W.J. Parker. Prediction of the Heat Release Rate of Douglas Fir. In *Fire Safety Science - Proceedings of the Second International Symposium*. Hemisphere Publishing Corporation, 1989. [Page 11.]
- [37] A. TenWolde, J.D. McNatt, and L. Krahn. Thermal Properties of Wood Panel Products Buildings. Report DOE / USDA-21697/ 1, USDA, Forest Products Laboratory, Madison, Wisconsin, 1988. [Page 11.]
- [38] K.W. Ragland, D.J. Aerts, and A.J. Baker. Properties of wood for combustion analysis. *Bioresource Technology*, 37(2):161–168, January 1991. ISSN 0960-8524. doi: 10.1016/0960-8524(91)90205-X. [Page 14.]
- [39] C. Di Blasi. Modeling and simulation of combustion processes of charring and non-charring solid fuels. *Progress in Energy and Combustion Science*, 19(1):71–104, January 1993. ISSN 0360-1285. doi: 10.1016/0360-1285(93)90022-7. [Page 15.]

- [40] X. Wang, C.M. Fleischmann, and M.J. Spearpoint. Parameterising study of tunnel experiment materials for application to the Fire Dynamics Simulator pyrolysis model. *Journal of Fire Sciences*, pages 1–25, 2016. doi: 10.1177/0734904116667738. [Page 16.]
- [41] A. Matala, S. Hostikka, and J. Mangs. Estimation of pyrolysis model parameters for solid materials using thermogravimetric data. In *Fire Safety Science - Proceedings of the 9th International Symposium*, pages 1213–1224, Karlsruhe, Germany, 2008. International Association for Fire Safety Science. doi: 10.3801/IAFSS.FSS.9-1213. [Pages 17 and 18.]
- [42] E. Sjöström. *Wood chemistry fundamentals and applications*. Academic Press, San Diego, 2nd edition edition, 1993. [Page 17.]
- [43] F. Richter, P. Kotsovinos, and G. Rein. The role of chemistry and physics in the charring of timber in realistic fires. *SFPE FPE Extra Issue*, (28), April 2018. URL https://sfpe.site-ym.com/default.asp?page=FPEExtraIssue28&_zs=HC01d1&_zl=rMOm4. [Page 18.]
- [44] Ian Pope, Juan P. Hidalgo, and José L. Torero. A correction method for thermal disturbances induced by thermocouples in a low-conductivity charring material. *Fire Safety Journal*, page 103077, May 2020. ISSN 0379-7112. doi: 10.1016/j.firesaf.2020.103077. URL <http://www.sciencedirect.com/science/article/pii/S0379711220300217>. [Pages 19, 20, and 21.]
- [45] J. König and L. Walleij. One-dimensional charring of timber exposed to standard and parametric fires in initially unprotected and postprotection situations. Technical Report 9908029, Swedish Institute for Wood Technology Research, Stockholm, Sweden, 1999. [Pages 19, 20, 22, and 23.]
- [46] Mayowa Akeem Azeez. Bamboo, Its Chemical Modification and Products. In Joshua Iseoluwa Orege ED1 - Abdul Khalil H.P.S., editor, *Bamboo*, page Ch. 3. IntechOpen, Rijeka, May 2018. ISBN 978-1-78923-231-8. doi: 10.5772/intechopen.76359. URL <https://doi.org/10.5772/intechopen.76359>. [Page 20.]
- [47] X. Li, X. Zhang, G. Hadjisophocleous, and C. McGregor. Experimental study of combustible and non-combustible construction in a natural fire. *Fire Technology*, 51:1447–1474, 2015. doi: 10.1007/s10694-014-0407-4. [Page 24.]
- [48] Nordic Wood Structures. *Technical Data - Nordic X-Lam*. 2013. URL http://nordic.ca/data/files/datasheet/file/T-S22_eTechnicalData.pdf. [Page 24.]
- [49] R.M. Hadden, A.I. Bartlett, J.P. Hidalgo, S. Santamaria, F. Wiesner, L.A. Bisby, S. Deeny, and B. Lane. Effects of exposed cross laminated timber on compartment fire dynamics. *Fire Safety Journal*, 91:480–489, 2017. ISSN 0379-7112. doi: 10.1016/j.firesaf.2017.03.074. [Page 24.]
- [50] C.J. McGregor. *Contribution of cross laminated timber panels to room fires*. Master of Applied Science Thesis, Carleton University, Ottawa, Canada, 2013. [Pages 24 and 29.]
- [51] J. Su, P. Lafrance, M. Hoehler, and M. Bundy. Fire safety challenges of tall wood buildings – Phase 2: Task 2 & 3 – Cross Laminated Timber Compartment Fire Tests. Report FPRF-2018-01, Fire Protection Research Foundation, Quincy, MA, 2018. [Pages 25, 27, 30, and 32.]

- [52] J. Su, P. Leroux, P. Lafrance, R. Berzins, K. Gratton, E. Gibbs, and M. Weinfurter. Fire testing of rooms with exposed wood surfaces in encapsulated mass timber construction. Report A1-012710.1, National Research Council of Canada, Ottawa, Canada, 2018. [Pages [28](#), [29](#), [30](#), and [32](#).]
- [53] APA - The Engineered Wood Association. ANSI/APA PRG 320-2018 Standard for performance-rated cross-laminated timber. American National Standard, APA - The Engineered Wood Association, Tacoma, WA, 2018. [Page [28](#).]
- [54] M.L. Janssens. Development of a fire performance assessment methodology for qualifying cross-laminated timber adhesives. Client Report SwRI Project No 01.23086.01.001a, Southwest Research Institute, San Antonio, Texas, 2017. [Page [29](#).]
- [55] D. Brandon, J. Schmid, J. Su, M. Hoehler, B. Östman, and A. Kimball. Experimental fire simulator for post-flashover compartment fires. In *Proceedings of the 10th International Conference on Structures in Fire*, Belfast, UK, 2018. [Page [31](#).]
- [56] S. Zelinka, L. Hasburgh, K. Bourne, D. Tucholski, and J. Ouellette. Compartment fire testing of a two-story cross laminated timber (CLT) building. General Technical Report FPL-GTR-247, U.S. Department of Agriculture, Forest Service, Forest Products Laboratory, Madison, Wisconsin, 2018. [Page [32](#).]
- [57] A.R. Medina Hevia. *Fire resistance of partially protected cross-laminated timber rooms*. Master of Engineering Thesis, Carleton University, Ottawa, Canada, 2014. [Page [32](#).]
- [58] V. Hankalin, T. Ahonen, and R. Raiko. On Thermal Properties of a Pyrolysing Wood Particle. In *Proceedings of Finnish-Swedish Flame Days 2009*, Tampere University of Technology, 2009. IFRF National Committees of Finland and Sweden. [Page [55](#).]

Appendices

A. Sensitivity of the post-flashover wood crib model in B-RISK to the plume entrainment algorithm used

For ventilation-controlled burning, the oxygen in the plume flow is used for combustion determining the ventilation-controlled heat release rate. As for pre-flashover burning, a single axisymmetric plume is assumed. However, it doesn't seem likely that a single axisymmetric plume developed using data from small preflashover fires would be a very good assumption for a post-flashover fire. The following discussion demonstrates the significance and sensitivity of B-RISK results for ventilation-controlled burning given this assumption and shows that the the results are relatively insensitive to the exact form of the plume correlation.

The mass flow in the plume comes from both the mass inflow through the vents and from any near vent mixing flow. The near vent mixing flow deposits gases from the upper layer into the lower layer and is the sole mechanism for contamination of the lower layer gases with combustion products. The mass fraction of oxygen in the vent inflow (coming from outside) will be ambient (0.231) while the mass fraction of oxygen in the near vent mixing flow (coming from the upper layer) will be largely depleted and close to zero after flashover or during ventilation controlled burning. These two flow streams mix together in the lower layer such that the oxygen mass fraction in the mixed lower layer lies between the two source flow values. The mass flows are illustrated in Figure A.1.

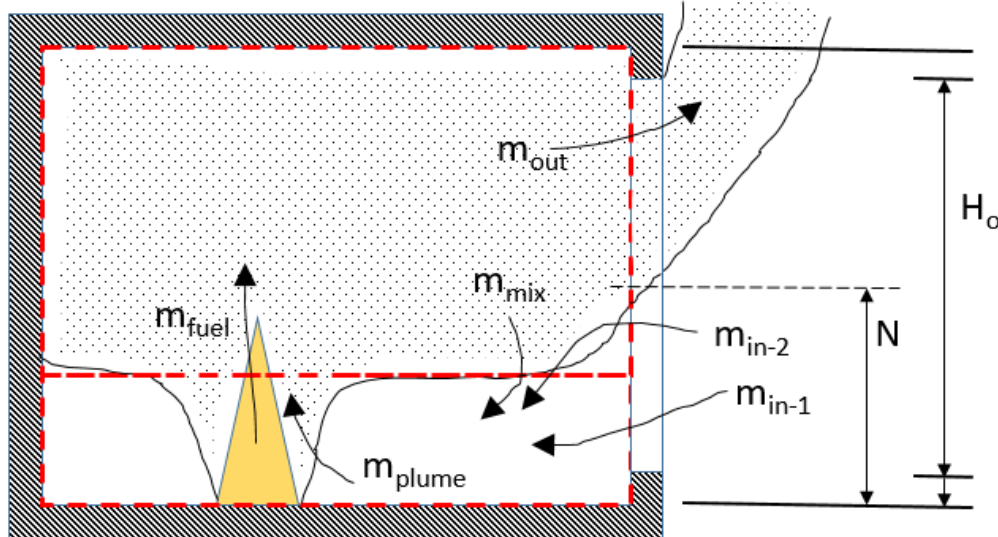


Figure A.1. Mass flows in compartment with opening with vent mixing term.

In B-RISK, after flashover and with the layer height close to the floor, the plume entrainment continues to be calculated using the McCaffrey "flaming" correlation [13] as follows, where \dot{Q}_{\max} is the maximum heat release rate that can be supported by the available oxygen supply:

$$\frac{\dot{m}_p}{\dot{Q}_{\max}} = 0.011 \left(\frac{z}{\dot{Q}_{\max}^{2/5}} \right)^{0.566} \quad (\text{A.1})$$

The mass flow of oxygen in the plume (kg-O₂/s) needed for complete combustion of

the fuel is given by:

$$\dot{m}_{O_2 \text{ needed}} = \frac{\dot{Q}_f}{13100} \quad (\text{A.2})$$

\dot{Q}_f is the theoretical, free-burning heat release rate. This equation is based on the observation that approximately 13,100 kJ of energy is released for every kg of oxygen consumed during the combustion reaction [19].

The actual mass flow of oxygen in the plume (kg-O₂/sec) is given by:

$$\dot{m}_{O_2 \text{ actual}} = \dot{m}_p Y_{O_{2,l}} C \quad (\text{A.3})$$

$Y_{O_{2,l}}$ is the mass fraction of oxygen in the lower layer. C is a coefficient described by Peacock et al [25] as given by Equation A.4 representing the fraction of fuel that can be burned with the available oxygen and varies between 0 and 1 to provide a smooth cut-off of the burning over a narrow range above the oxygen limit. An oxygen limit of 10% by volume is assumed with the corresponding mass fraction given in Equation A.5.

$$C = \frac{\tanh(800(Y_{O_{2,l}} - Y_{\text{lim}}) - 4) + 1}{2} \quad (\text{A.4})$$

$$Y_{\text{limit}} = 0.1 \frac{MW_{O_2}}{MW_{l,\text{avg}}} \quad (\text{A.5})$$

When cool air flows into the room through a wall vent, it is assumed to entrain some of the upper layer gases from the upper layer into the lower layer. This can result in a blurring of the sharp distinction between the two stratified gas layers. The near vent mixing correlation developed by Utiskul has been applied where the incoming cold air behaves like a jet entering the vent with a characteristic velocity and diffusing downward because of buoyancy [11]. While the cooler air descends, the surrounding hot gas is entrained with a velocity that is proportional to the incoming flow characteristic velocity. An equation for the ratio of mass entrained to the total incoming mass flow was developed by Utiskul and single-vent compartment fire experiments were conducted to establish the correlation for the mixing at the quasi-steady state. The correlation exhibited a linear relationship up to an apparent asymptote for the mixing ratio of about 1.3 [11]. This vent mixing mass flow, taken from the upper layer and added to the lower layer, applies both to vents to the exterior and vents to adjacent rooms.

Since the mass flow in the plume depends on the fire heat release rate, and the heat release rate depends on the oxygen available in the plume, these calculations are done iteratively at each time step until the difference between successive calculations of the oxygen constrained heat release rate is sufficiently small. Ultimately the inflow of air to the compartment determines the heat released inside the compartment rather than the total mass flow in the plume. This is demonstrated by an example.

Example

Consider a room 8.6 m long \times 5.9 m wide \times 3.9 m high, with an opening 2.2 m high \times 1.906 m wide. The fuel is wood cribs 285 MJ/m² (floor area basis). A simple estimate of the ventilation limit for this compartment using $\dot{Q}_{\text{max}} = 1500 A_o \sqrt{h_o}$ is 9329 kW.

Simulations to test the sensitivity of the compartment mass flows and heat release rate to the magnitude of the plume flow were run. The plume flow calculated using Equation A.1 for the McCaffrey flaming correlation was multiplied by factors of 0.5 and 2.0.

Figure A.2 compares the calculated plume flow using the McCaffrey correlation [13] for the flaming region (black line) with that obtained by multiplying the right hand side of Equation A.1 by a factor of 0.5 (blue) and 2.0 (red) respectively. The three cases clearly result in a different calculated total plume flow, but they are not one-half and double the original value because the plume flow and layer height are dependent on each other. If the plume flow is increased, the upper layer volume increases lowering the layer height (and reducing entrainment and plume flow). The plume flow effect on the calculated layer height is shown in Figure A.3.

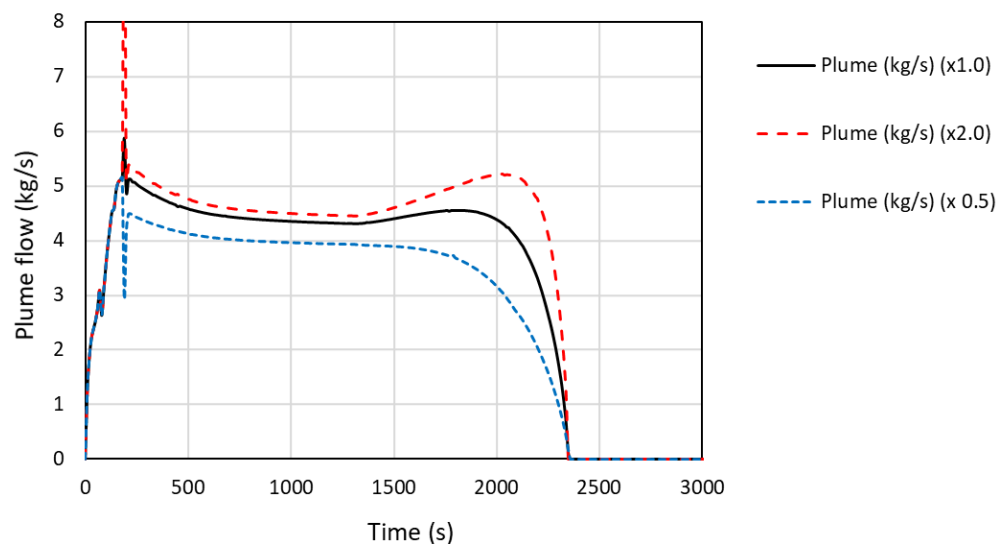


Figure A.2. Plume entrainment, flaming region.

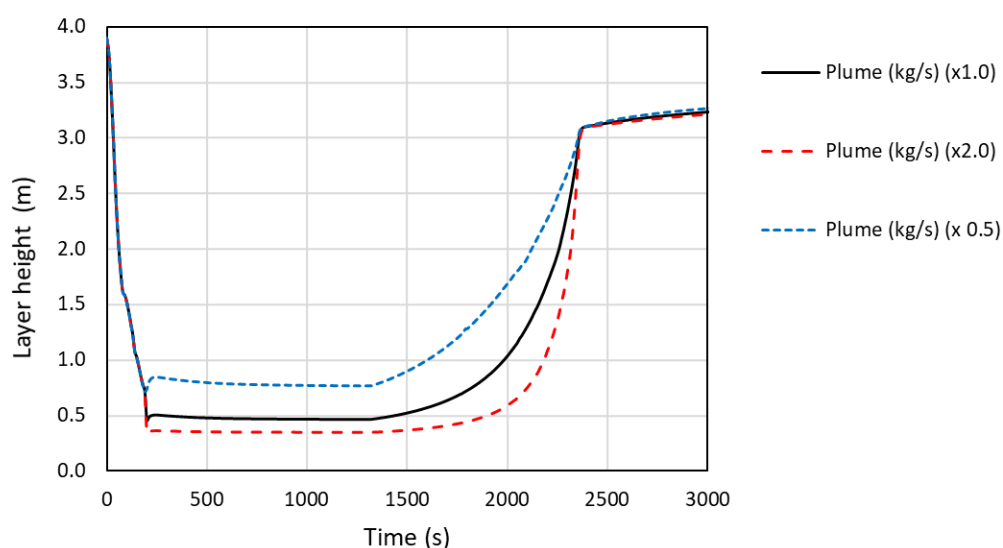


Figure A.3. Effect of plume flow on the layer height.

In addition, if the burning is oxygen-constrained the rate of heat release is determined by the oxygen mass flow in the plume which in turn is dependent on the rate of heat release. If the plume flow increases (assuming the same mass fraction of oxygen in the plume) the rate of heat release would also increase.

Now compare the calculated heat release rate in the compartment shown in [Figure A.4](#) for the three cases. The oxygen-constrained heat release rate is identical. This means that the oxygen mass flow in plume must be the same in each case even though the total plume flow is different (as per [Figure A.2](#)). This requires the oxygen mass fraction feeding the plume to be also different. For completeness, [Figure A.5](#) shows the effect of the plume entrainment on the upper layer temperatures.

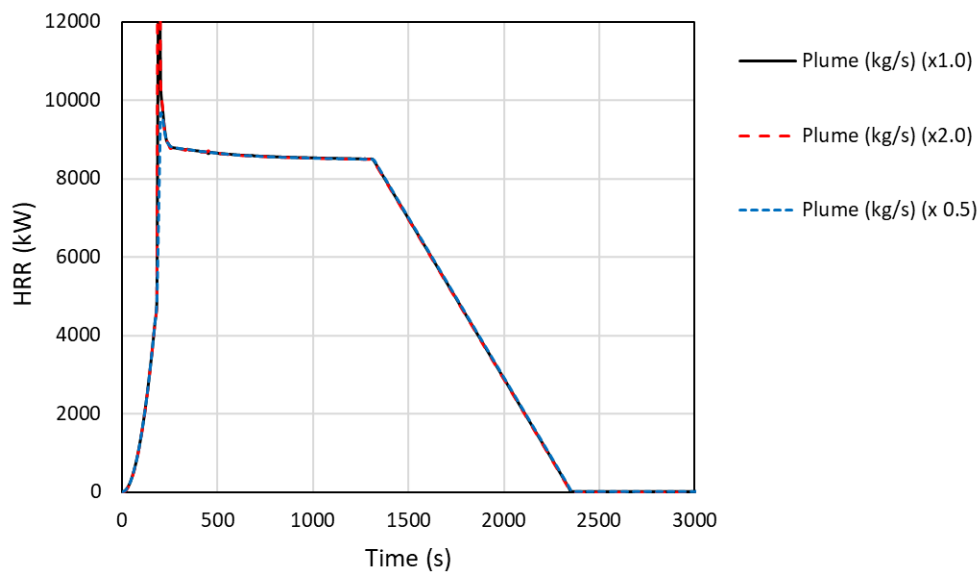


Figure A.4. Effect of plume flow on the heat release rate.

Consider a snapshot of the mass flows in the compartment at 1000 seconds for each case. In all three cases the calculated oxygen mass flow in the plume is calculated as 0.65 kg/s as shown below.

At 1000 sec (using McCaffrey plume $\times 1.0$)

Vent flow output from B-RISK is shown in [Figure A.6](#). The corresponding flow schematic is shown in [Figure A.9](#). The mass flow of oxygen in the plume is calculated as follows:

$$\begin{aligned}
 \dot{m}_{O_2} = \dot{m}_p Y_{O_{2,l}} &= \dot{m}_p V_{O_{2,l}} \frac{MW_{O_2}}{MW_{l,avg}} \\
 &= \dot{m}_p V_{O_{2,l}} \frac{MW_{O_2}}{MW_{l,avg}} \\
 &= 4.355 \times \frac{13.6}{100} \times \frac{32}{29.19} = 0.65 \text{ kg/s}
 \end{aligned}
 \tag{A.6}$$

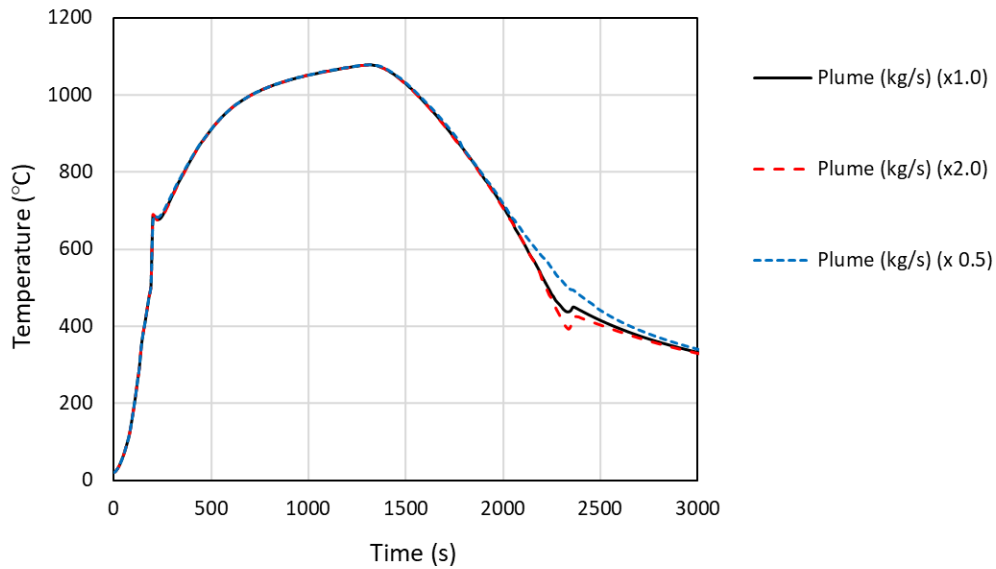


Figure A.5. Effect of plume flow on the calculated upper layer gas temperature.

At 1000 sec (using McCaffrey plume $\times 2.0$)

Vent flow output from B-RISK is shown in [Figure A.7](#). The corresponding flow schematic is shown in [Figure A.10](#). The mass flow of oxygen in the plume is calculated as follows:

$$\begin{aligned}
 \dot{m}_{O_2} &= \dot{m}_p Y_{O_2,l} = \dot{m}_p V_{O_2,l} \frac{MW_{O_2}}{MW_{l,avg}} \\
 &= \dot{m}_p V_{O_2,l} \frac{MW_{O_2}}{MW_{l,avg}} \\
 &= 4.499 \times \frac{13.2}{100} \times \frac{32}{29.205} = 0.65 \text{ kg/s}
 \end{aligned} \tag{A.7}$$

At 1000 sec (using McCaffrey plume $\times 0.5$)

Vent flow output from B-RISK is shown in [Figure A.8](#). The corresponding flow schematic is shown in [Figure A.11](#). The mass flow of oxygen in the plume is calculated as follows:

$$\begin{aligned}
 \dot{m}_{O_2} &= m_p Y_{O_2,l} = m_p V_{O_2,l} \frac{MW_{O_2}}{MW_{l,avg}} \\
 &= m_p V_{O_2,l} \frac{MW_{O_2}}{MW_{l,avg}} \\
 &= 3.961 \times \frac{14.9}{100} \times \frac{32}{29.127} = 0.65 \text{ kg/s}
 \end{aligned} \tag{A.8}$$

Wall Vent Flows						
Time(s)	from-room	to-room	vent#	#slabs	elevation (m)	ventflow(kg/s)
0	1	2	1	1	0.900 to 3.100	1.238
1000	1	2	1	2	1.683 to 3.100 0.900 to 1.683	3.259 -2.807
2000	1	2	1	3	1.773 to 3.100 1.034 to 1.773 0.900 to 1.034	3.228 -2.449 -0.696
3000	1	2	1	2	1.949 to 3.100 0.900 to 1.949	2.501 -2.529

Figure A.6. B-RISK Wall vent flow output with McCaffrey plume flow $\times 1.0$.

Wall Vent Flows						
Time(s)	from-room	to-room	vent#	#slabs	elevation (m)	ventflow(kg/s)
0	1	2	1	1	0.900 to 3.100	1.238
1000	1	2	1	2	1.683 to 3.100 0.900 to 1.683	3.259 -2.806
2000	1	2	1	2	1.773 to 3.100 0.900 to 1.773	3.232 -3.143
3000	1	2	1	2	1.949 to 3.100 0.900 to 1.949	2.487 -2.513

Figure A.7. B-RISK Wall vent flow output with McCaffrey plume flow $\times 2.0$.

Wall Vent Flows						
Time(s)	from-room	to-room	vent#	#slabs	elevation (m)	ventflow(kg/s)
0	1	2	1	1	0.900 to 3.100	1.238
1000	1	2	1	2	1.683 to 3.100 0.900 to 1.683	3.258 -2.807
2000	1	2	1	3	1.791 to 3.100 1.689 to 1.791 0.900 to 1.689	3.157 -0.125 -3.018
3000	1	2	1	2	1.947 to 3.100 0.900 to 1.947	2.537 -2.567

Figure A.8. B-RISK Wall vent flow output with McCaffrey plume flow $\times 0.5$.

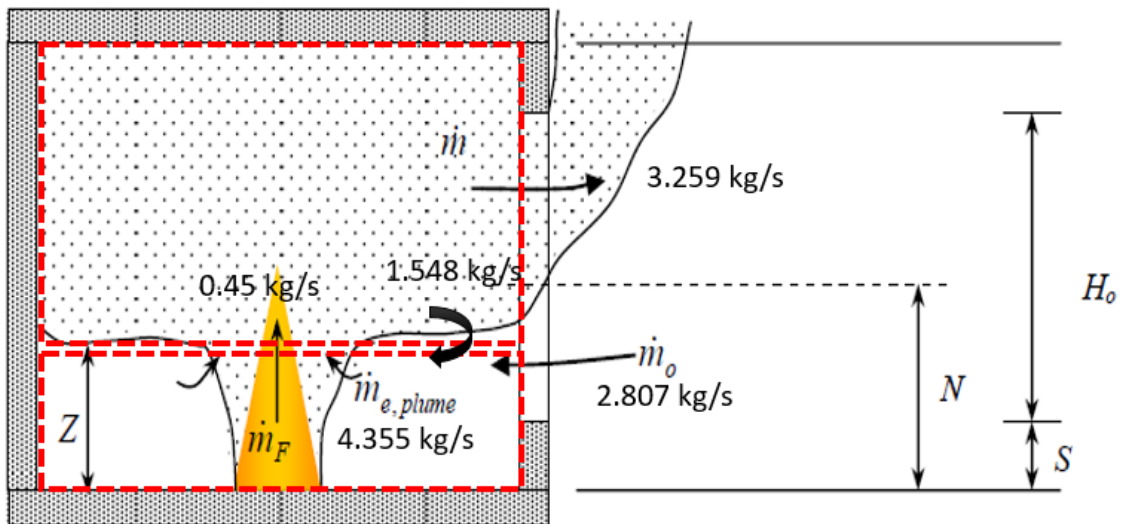


Figure A.9. Flow schematic at 1000 s with McCaffrey plume flow $\times 1.0$.

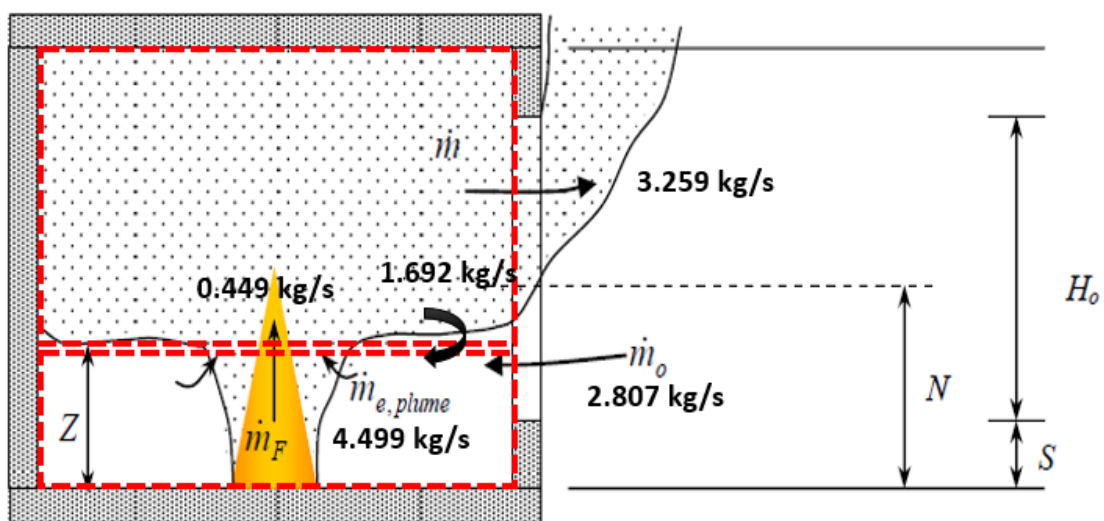


Figure A.10. Flow schematic at 1000 s with McCaffrey plume flow $\times 2.0$.

54

B. Mass timber simple GE submodel

B.1 Description

The mass timber simple GE submodel provides an alternative, simpler means of accounting for the pyrolysis of the mass timber surfaces as they char. The preflashover fire and combustion of the moveable fire load (contents) is as previously described in [section 2](#) and after flashover are assumed to burn as wood cribs with a mass corresponding to the unburned fuel in the room at flashover.

A flow chart illustrating the coupling of moveable fire load and the contribution of the mass timber when the simple GE pyrolysis submodel is used is shown in [Figure B.1](#).

The general form of the heat conduction calculations through the walls are as previously described in [subsection 3.1](#). At any given time, each finite difference element or slice is designated 'wood' or 'char' depending on whether it has previously reached the designated char temperature.

The specific heat of wood and char are as described in [subsection 4.5](#). The density of wood is taken as a constant specified by the user, while the density of char is determined from:

$$\rho_c = \frac{0.63\rho_w}{1 + u} \quad (\text{B.1})$$

where ρ_w is the density of the wood at ambient and u is the moisture content by mass.

Hankalin et al. [58] proposed the temperature dependent thermal conductivity values in [Equation B.2](#) to [Equation B.4](#) for a pyrolysing wood particle where thermal conductivity at ambient temperature is given as the average of the longitudinal and radial directions so may be higher than actually applicable for this application. Although Hankalin indicated [Equation B.4](#) applied up to 923 K, it has been used for higher temperatures (up to 1200°C) here. Furthermore, the thermal conductivity of 'char' is treated as being non-reversible such that the maximum temperature reached is used for any subsequent determination of thermal conductivity. Any wood that has reached a minimum temperature of 300°C is considered to be 'char'.

$$k = 0.285 \text{ for } T \leq 473 \text{ K} \quad (\text{B.2})$$

$$k = -0.617 + 0.0038T - 4 \times 10^{-6}T^2 \text{ for } 473 < T \leq 663 \text{ K} \quad (\text{B.3})$$

$$k = 4.429 \times 10^{-2} + 1.477 \times 10^{-4}T \text{ for } 663 < T \leq 923 \text{ K} \quad (\text{B.4})$$

The incident heat flux to the enclosure surfaces are calculated by [Equation 14](#) to [Equation 17](#). The depth below the surface of the isotherm within the CLT surface corresponding to the char temperature (typically assumed as 300 °C) is assumed to have pyrolysed. At each time step the change in the char depth from the previous time step is determined and the corresponding mass is determined. This is converted to an equivalent fire load energy per unit floor area and is added to the contents fuel load for use in subsequent calculations for the contents pyrolysis.

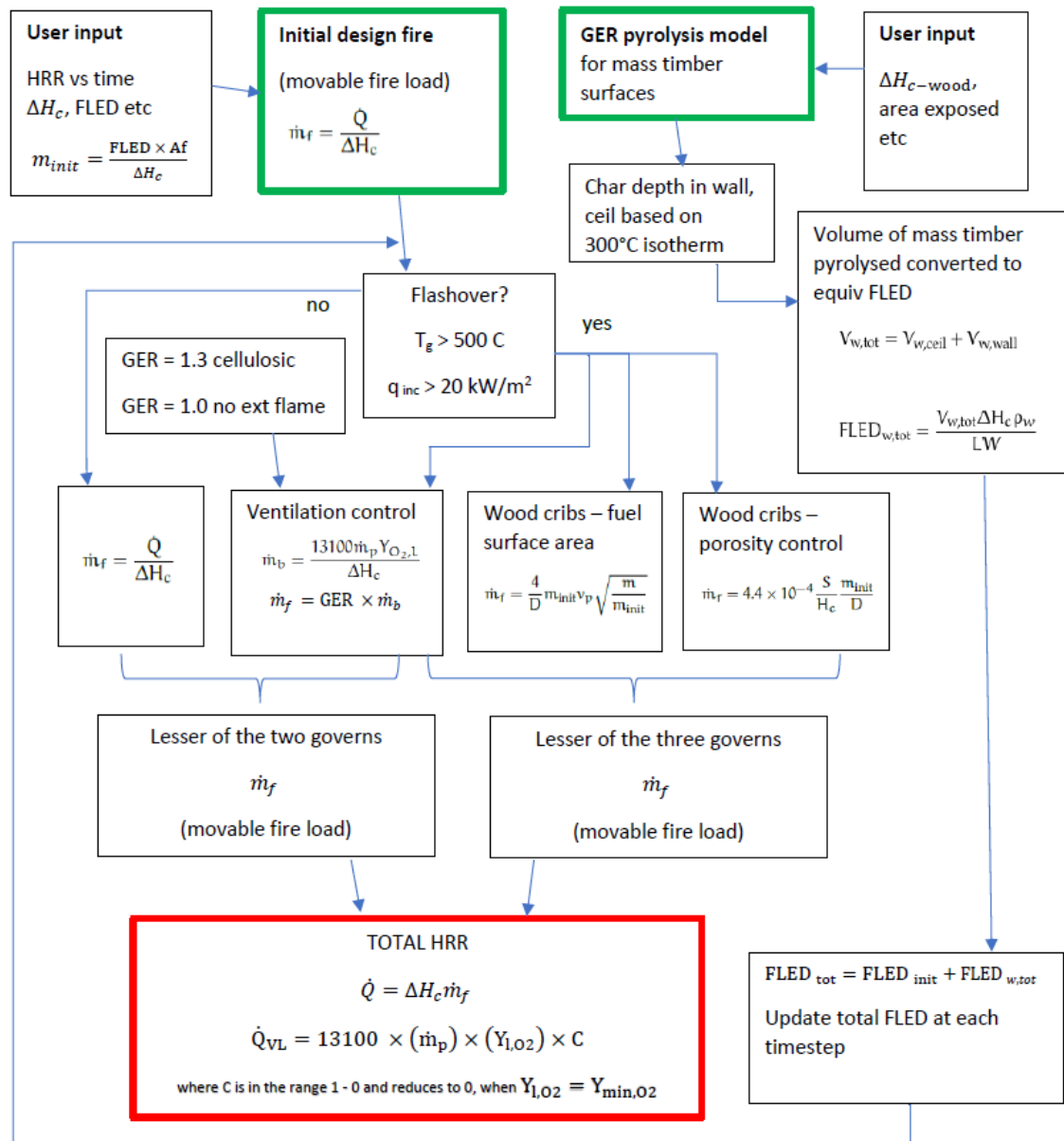


Figure B.1. Flow chart for the moveable fire load coupled with the simple GE submodel for mass timber [5].

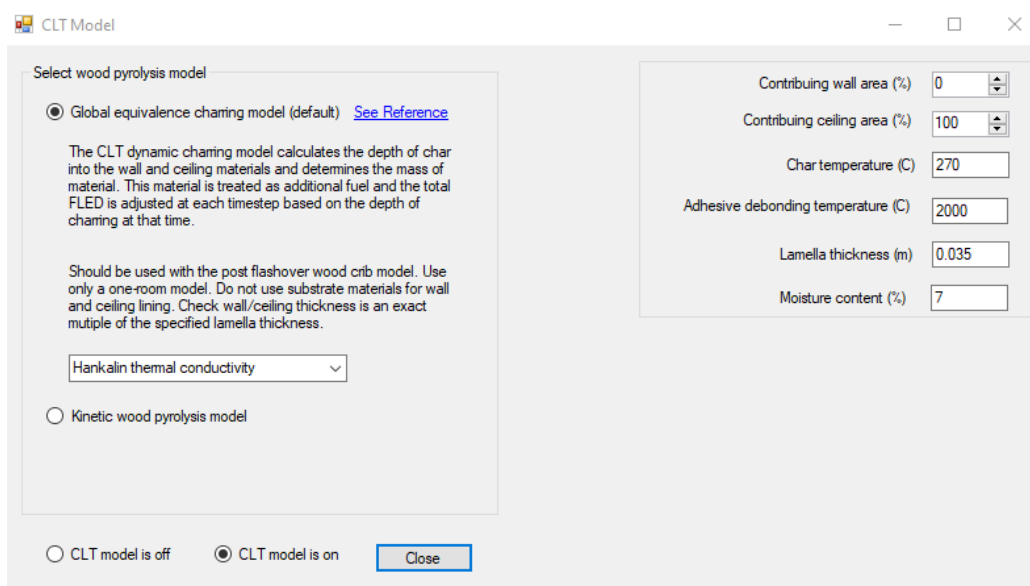
B.2 Instructions for the mass timber simple GE submodel

This section describes how to set up and use the simple GE submodel for a fire in an exposed mass timber compartment.

The room materials and thermal properties are set by following Steps 1 to 3 in [subsection 7.1](#) as for the kinetic submodel.

1. As shown in [Figure B.2](#), to use the mass timber simple GE model the **CLT model is on** radio button option should be selected along with the **Global equivalence charring model** radio button option.

2. The percentage of wall and ceiling area comprising exposed mass timber should be entered. The char temperature can be specified. For this submodel, it is recommended that a char temperature of 270 °C be used instead of 300 °C for added conservatism.
3. The lamella thickness should be entered. It must be divisible into the specified wall thickness. In this example for a 140 mm thick wall or ceiling element there will be four lamella each 0.035 m thick.
4. The moisture content as a percentage by mass is entered.
5. The solver settings are reached using the **Misc Settings, Solvers** menu item with the form shown in [Figure 26](#). It is recommended that the number of nodes per layer for the wall and ceiling be set such that the finite element thickness is 1 mm. In the example shown for a 140 mm thick wall with each lamella 35 mm thick, the number of nodes for each lamella is then 36.
6. The mass timber pyrolysis model is used in conjunction with the postflashover sub-model with the settings reached from the **Misc Settings, Postflashover Behaviour** menu item as shown in [Figure 27](#). The option for **Use Wood Crib Postflashover Model** should be set to **yes**. To ensure a more conservative prediction, it is suggested that the Excess Fuel Factor be set equal to 1. This will mean all the fuel will burn inside the room with no external burning.
7. Once the model is set up and the preceding parameters for the pyrolysis model have been set, the model is run as usual using the **Start Simulation** menu item.
8. Output from the model for the char depth can be obtained from the **Single Run Graphs, Surface Internal Temperatures, Wall - char depth** menu item as shown in [Figure 28](#) and [Figure 29](#).



The screenshot shows the 'CLT Model' dialog box with the following settings:

- Select wood pyrolysis model:**
 - ☒ Global equivalence charring model (default) [See Reference](#)

The CLT dynamic charring model calculates the depth of char into the wall and ceiling materials and determines the mass of material. This material is treated as additional fuel and the total FLED is adjusted at each timestep based on the depth of charring at that time.

Should be used with the post flashover wood crib model. Use only a one-room model. Do not use substrate materials for wall and ceiling lining. Check wall/ceiling thickness is an exact multiple of the specified lamella thickness.

Hankalin thermal conductivity
 - ☐ Kinetic wood pyrolysis model
- Contributing wall area (%):** 0
- Contributing ceiling area (%):** 100
- Char temperature (C):** 270
- Adhesive debonding temperature (C):** 2000
- Lamella thickness (m):** 0.035
- Moisture content (%):** 7
- CLT model is off:** ☐ **CLT model is on:** ☒ **Close**

Figure B.2. Parameters for the mass timber simple GE model.